UCL Université catholique de Louvain

École polytechnique de Louvain (EPL)

epl

Optimal Design and Control for an Artificial Leg

Energy Consumption Minimization

Dissertation presented by
Matthias TUMMERS

for obtaining the Master's degree in
Biomedical Engineering
Option: Biomechanics and medical robotics

Supervisor
Renaud RONSSE

Readers
Bruno DEHEZ, Laurent DELANNAY , Christophe EVERARTS

Academic year 2015-2016

Acknowledgements

I would like to thank everyone that contributed and helped me in the completion of this work. Realizing it has been a real enriching journey for me, but it would have been definitely impossible without the support of all of you.

In the first place I am particularly grateful to Professor Renaud Ronsse who guided me as supervisor during the realization of this venture. He has been all along a source of inspiration and a tough, yet always sound, challenger of my work and progress.

My thanks also go to Christophe Everarts who co-supervised my work. The numerous progress sessions we had together and his continuous support were really material to the achievement of this project.

I also want to thank all the faculty of the École Polytechnique de Louvain of the UCL and the École Polytechnique de Montreal. The teaching of the many different biomedical and general engineering disciplines they provided me this last five years was more than useful in attaining the result presented here.

Finally I would like to thank my family and friends for the unconditional support and encouragements they gave me from the beginning till the end.

Abstract

This work proposes the design of a model for a new IVT based mechanism for an active transfemoral ankle-knee prosthesis. Most importantly, it accurately models the energy losses during the energy transfers in the prosthesis. Further, a control architecture is developed and tuned to torque-control the prosthesis in various tasks while minimising the total energy consumption of the actuators. Additionally, a simplified dynamic model of the ankle is used to investigate the behaviour of the prosthesis in a real situation.

The models and controllers were validated with experimental results.

Contents

List of Symbols

χ Main motor gear ratio

Δt_{step} Duration of one step in the considered task

η Efficiency of the considered mechanical element (see Equation (6.2))

η_g Efficiency of the main motor gear

η_r Efficiency capturing the energy lost due to friction in the movement of the IVT rings

η_{CVT} Efficiency of the CVT of the IVT

$\eta_{IVT,\,ankle}$ Mean weighted efficiency of the IVT at the ankle joint, weighted in function of the transmission ratio

$\eta_{IVT,\,knee}$ Mean weighted efficiency of the IVT at the knee joint, weighted in function of the transmission ratio

η_{LS} Efficiency of the lead screw

η_{PG} Efficiency of the planetary gear of the IVT

ω_g Angular velocity of the main motor gear output shaft

ω_i Angular velocity of the IVT motor at the IVT of the considered joint

ω_m Main motor velocity

ω_s Spring deformation rate

ω_w Rate at which the spring is unwound/rewound

ω_{ankle} Ankle joint velocity

ω_{an} Angular velocity of the annulus of a planetary gear train

ω_{ca} Angular velocity of the planet carrier of a planetary gear train

ω_{knee} Knee joint velocity

ω_{su} Angular velocity of the sun gear of a planetary gear train

$\omega_{w,\,ankle}$ Rate at which the spring would be unwound/rewound if the ankle was the only joint (i.e. no differential between spring and IVT); product of ω_{ankle} and n_{ankle}

$\omega_{w,\,knee}$ Rate at which the spring would be unwound/rewound if the knee was the only joint (i.e. no differential between spring and IVT); product of ω_{knee} and n_{knee}

$\overline{P_s}$ Mean spring power output for the considered task (i.e. the net energy the spring produces at the joints side for the considered task divided by Δt_{step})

θ_i Angular position of the IVT motor at the IVT of the considered joint

θ_s Spring deformation angle

θ_{ankle} Angular position of the ankle joint with respect to Figure 8.1

ε_E Error on the spring energy: difference between E_r and E_s

ε_T Error on the output torque at the considered joint

ε_x Error on the IVT ring position of the IVT at the considered joint

B_i IVT motors viscous damping constant

B_m Main motor viscous damping constant

B_{ankle} Viscous damping constant in the dynamic model of the ankle joint

C_m Main motor speed torque gradient

E_r Reference for the spring energy

E_s Spring energy

F_r Reaction force of the ground on the ankle due to the body weight

I Inertia of the body with respect to the ankle

I_i Current in the IVT motor at the IVT of the considered joint

I_m Current in the main motor

J_eq IVT motors equivalent inertia, considering the lead screw and the ring in addition to the motor's rotor

J_i IVT motors rotor inertia

J_m Main motor rotor inertia

k Spring stiffness

K_i IVT motors torque constant

K_m Main motor torque constant

K_p Proportional gain of the main motor controller

k_{LS} Rotational motion into linear motion coefficient of the lead screw between the IVT motors and the rings of the IVT's

L Distance between the centre of mass and the ankle joint in the sagittal plane

l Length of the foot (i.e. distance between the contact point with the ground and the ankle joint in the sagittal plane)

L_i IVT motors terminal inductance

L_m Main motor

m Total mass of the ring of the IVT

n_d Desired transmission ratio at the IVT of the considered joint

N_s Number of turns in the spring

n_{ankle} Variable transmission ratio at the IVT at the ankle joint

N_{an} Number of teeth in the annulus of a planetary gear train

n_{CVT} Transmission ratio of a CVT

n_{IVT} Transmission ratio of an IVT

n_{knee} Variable transmission ratio at the IVT at the knee joint

$n_{PG,\,ankle}$ Transmission ratio of the planetary gear train of the IVT at the ankle joint

$n_{PG,\,knee}$ Transmission ratio of the planetary gear train of the IVT at the knee joint

n_{PG} Transmission ratio of a planetary gear train

N_{su} Number of teeth in the sun gear of a planetary gear train

P_m Main motor mechanical power output

P_s Spring power (i.e. the power the spring produces or absorbs at the joints side, $\omega_w T_s$)

R_i IVT motors terminal resistance

R_m Main motor terminal resistance

rr Ratio range (defined for a CVT or an IVT)

T_m Main motor torque output

T_s Spring torque

T_{ankle} Prosthesis output torque at the ankle joint

T_{an} Torque in the annulus of a planetary gear train

$T_{av,\,ankle}$ Available torque at the spring side of the IVT at the ankle joint

$T_{av,\,knee}$ Available torque at the spring side of the IVT at the knee joint

T_{ca} Torque in the planet carrier of a planetary gear train

$T_{d,\,ankle}$ Desired prosthesis output torque at the ankle joint

$T_{d,\,knee}$ Desired prosthesis output torque at the knee joint

T_{knee} Prosthesis output torque at the knee joint

T_{su} Torque in the sun gear of a planetary gear train

U_i Voltage to the the IVT motor at the IVT of the considered joint; IVT motor command

U_m Voltage to the main motor; main motor command

U_r Reference voltage in to the main motor

x IVT ring position of the IVT at the considered joint

x_d Desired IVT ring position of the IVT at the considered joint

List of Figures

Introduction

Perspective and needs

The number of amputees in the worldwide population is appallingly striking. Various sources show that amputation has a significant incidence and high prevalence, [4], [1]. For example [4] reports a worldwide incidence of amputation of 1.5 for 1000. Hence there are more than 1 million annual limb amputations globally — one every 30 seconds.

The reasons for amputation are wide and various. Various diseases such as poor blood circulation caused mainly by diabetes or other arterial diseases lead to numerous amputations of foot and part of legs [2]. Soldiers get injured and disabled through the loss of one of their limbs in the too many wars and fights the world is still facing. Unexploded ordnances (UXO's) and anti-personnel mines, although their use is banned through international treaties, yearly claim their toll of innocent victims (for the description of this subject see for example [3]). Accidents of various types — occupational, professional, circulation accidents, bite by snakes, extreme sports, etc. — also add to the number of people getting disabled by amputation.

Although medical doctors try and do their best to avoid to recourse to the extreme solution of amputation, a lot of people still need to learn and live with the handicap of the loss of one of their limbs.

It is hence very understandable that one of the main focuses of the emerging biomedical engineering sciences these last years has been the quest for even better solutions to relieve these disabled people from their handicap.

Prostheses for the lower limb

Significant research and development have already been performed in the case of lower limb prostheses. The first prostheses were mere passive and simple devices enabling the amputee to regain equilibrium and some form of mobility generally with the help of crutches. Evolution was more oriented towards making the prosthesis comfortable (form and weight) and sustainable.

These last decades have witnessed a considerable evolution in the design of these prostheses aiming at making them more functional by taking into consideration the dynamic aspects of the normal gait cycle and making the prosthesis more integrated in it. Very soon the issue of energy management arose especially for transfemoral prosthesis.

This issue has been tackled in different ways either by passive prostheses or by active prostheses. Some passive designs store energy during some phases of the gait cycle and restore it at others but with the limitation that in any case a net external energy has to be provided to the prosthesis. Active prosthesis on the other hand, while solving the net energy issue, camp with the difficulty of compactness and weight increase due to the presence of energy packs (batteries) and motors.

Objective of this study

This work will in the case of an active type of prosthesis aim at optimizing the energy management hence not only allowing for a more compact solution but also considerably enhancing its autonomy. To do so, a model needs first to be set-up. This model takes into account the energy and power flows and transfers in the specific prosthesis under consideration during the gait cycle. The model also considers the efficiencies of different parts of the prototype (e.g. friction effects in the mechanisms). Using this model, a control system is then designed allowing for the minimization of energy consumption. Finally the impact on the joint dynamics of the obtained torque tracking is analysed.

Chapter 1

How the human gait influences the design of prostheses

1.1 The human gait analysis

Walking is a cyclic repetition of strides which are composed of left and right steps. Each stride can in turn be divided into the stance phase and the swing phase for one of the legs.

During the stance phase, which takes about 60% of the stride, the foot is in contact with the ground. It starts with the heel strike, then the weight is gradually transferred from the other leg before balancing forward around the foot and ankle. This is called the controlled dorsiflexion because the movement in the foot relative to the leg is in the direction of the dorsal side of the foot. The stance phase ends with a push-off of the ankle (and the knee finishing its extension) driving the body forward. This is called the powered plantar flexion because the movement of the foot relative to the leg is in the direction of the plantar side of the foot.

The swing phase, which takes about 40% of the stride, is when the foot does not touch the ground. It follows the stance phase and starts when the foot leaves the ground after the push-off. There is then a flexion in the knee joint to bring the leg forward for the next step. The swing phase ends when the heal strikes the ground, which brings us back to the stance phase.

This complex pattern cares for large fluctuations in the ankle and knee angular velocities and torques, resulting in non trivial power profiles for both joints.

1.2 Analysis of the power profiles of the lower limb joints

Before going further, it should be stated that all the data that is used in this project comes from the data collected by Riener et al. [20] in their research for investigating the bio-mechanics and motor coordination in humans during stair climbing at different inclinations.

Figure 1.1 shows the power profiles for level ground walking for the ankle and the knee joint. The red areas represent the produced[1] energy at the joints whereas the green areas represent the dissipated energy. This figure makes it clear that, for both joints, there are phases when power is produced and phases where power is dissipated. In particular, at the ankle:

- during the swing phase almost no power is produced nor dissipated;
- during the first part of the stance phase, the controlled dorsiflexion, energy is dissipated to prevent the body from falling forward; and
- during the second part of the stance phase, the powered plantar flexion, energy is produced to propel the body forward.

[1] Production of energy means that joint has to produce energy in order to induce motion to the body (i.e. a production of energy from the joint to the outside world). Conversely, dissipation of energy means that the joint absorbs energy from the body's motion (i.e. an absorption of energy from the outside world by the joint).

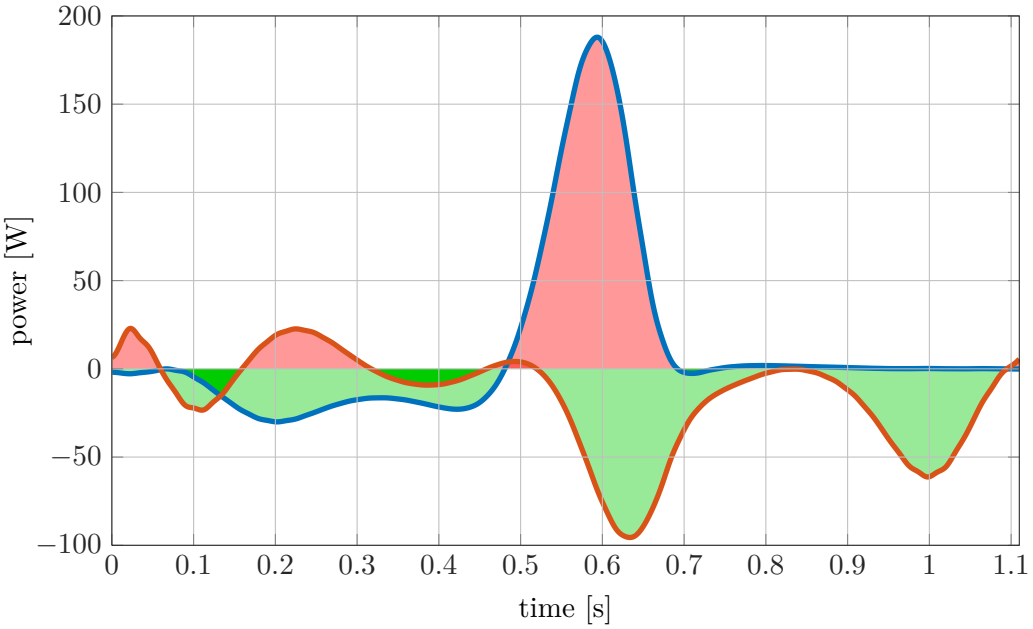

Figure 1.1: Power developed by the ankle (blue line) and the knee (red line) during one stride of level-ground walking. The red shaded areas represent energy produced at the joints, the green shaded areas represent dissipated energy at the joints.

In total, more power is produced than dissipated, making the net energy production at the ankle positive. For the knee joint:

- during the swing phase, energy is dissipated by braking the forward movement of the leg; and
- during the stance phase, the knee both produces and dissipates energy.

In total, more power is dissipated than produced which makes the net energy production at the knee joint negative.

These power profiles have a predominating impact on the behaviour of transfemoral lower limb prostheses.

1.3 Impact of the power profiles on the design of lower limb prostheses

The first thing we want to conclude from the power profiles analysis is that, during locomotion, both joints produce power. This explains why some passive prosthesis (the ones in which no power flows occur) fail to reproduce a normal walking gait.

The second thing, is that the net energy produced by the knee is negative whereas the net energy produced by the ankle is positive. This explains how a prosthesis that uses compliant elements to store and release energy at both joints could potentially reproduce a normal walking pattern at the knee joint but not at the ankle joint. A solution is to transfer energy harvested at the knee to the ankle. Indeed, the total net energy consumed (all green areas minus all red areas in Figure 1.1) at both joints is negative. Several prostheses are based on this approach:

- The WalkMECH prosthesis from the University of Twente: the mechanism is based on three different elements, which are responsible of the energetic coupling between the knee and ankle joints. A linkage system that couples the knee and ankle joints; an elastic

element that energetically couples the knee and ankle joints and a linear elastic element which is responsible for the absorption of the energy dissipated at the ankle, [6], [26].

- The HEKTA prosthesis from the Vrije Universiteit Brussel: the name is an acronym that stands for Harvest Energy from the Knee and Transfer it to the Ankle which speaks for itself. This prosthesis uses two energetic couplings: a spring and a cable that is connected and disconnected at different instances of the stride; and a stance spring that is disconnected during the swing phase, [19].

In practice however, energy losses occur and it is not yet possible to harvest and release enough energy to obtain a normal walking gait with these prostheses. The solution is to turn to active (or powered) prostheses. These involve one or more actuators to compensate for the lacking power. The project led by M. Goldfarb at the Vanderbilt University of an active transfemoral lower limb prostheses uses an energy storing element and provides power with actuators to fill in the needs. The prosthesis uses two actuators, one standard actuator at the knee and a series-elastic actuator at the ankle (see Section 2.1). However this prototype can provide the needed power at the joints, it has a high energy consumption which makes it a non viable solution for prolonged use, [23]. The control of this prosthesis is studied in the articles: [27], [14], [24], and [17].

The present work focuses on a mechanism for an active prosthesis that stores energy from both joints in a compliant element and releases it independently at the two joints. To compensate for the energy losses that occur when the power flows through mechanical elements, an actuator supplies the additionally needed energy to the same compliant element.

1.4 Climbing and descending stairs

In this work the prosthesis behaviour in the task of level ground walking is analysed but also in the tasks of climbing and descending stairs. Indeed, the power profiles are different for these tasks, and thus, the amount of energy stored and released is not the same. This has an impact on the design of the prosthesis as well as on its control.

As the research of Riener et al. [20] focusses on different stair inclinations, their data contains the measurements for these different inclinations, in this work however, only the data for the "normal" inclination is used.

Chapter 2

Compliant lower limb prosthesis

2.1 From Series Elastic Actuators ...

A Series Elastic Actuator (SEA) is a serial connection of a standard actuator with an compliant element. These actuators are suited for cyclic tasks that involve power production and dissipation. Indeed, during the power dissipation phase of the cycle, energy is stored in the elastic element and during the the power production phase the stored energy is released. This makes this kind of actuators particularly suitable for the task of human locomotion that involves power profiles with large fluctuations in positive and negative values. Several ankle prostheses exploit this principle, some examples are:

- The SPARKy prosthesis from the the Arizona State University: SPARKy stands for Spring Ankle with Regenerative Kinetics, which speaks for itself. The design uses a SEA attached between the heel and the leg that provides the necessary power, [7], [16].
- Herr's Bionic ankle–foot prosthesis from the Massachusetts Institute of Technology: its working principle consists of loading a spring during the controlled dorsiflexion phase and to activate a torque source in parallel when peak power is needed. [15]
- The AMP-FOOT from the Vrije Universiteit Brussel: the Ankle Mimicking Prosthesis uses a low power actuator which stores energy in springs during the complete stance phase that can be released at push-off, thanks to the use of a locking system. This reduces the size and weight of the actuator [10].

The capacity to store and release energy of these prostheses proves very effective for flattening the motor's power profile with respect to the one transmitted to the load. As one of the key factors influencing the size of a motor is its peak power, this is a very interesting result. On top of that, utilizing SEA's in lower limb prosthesis has also proved other advantages. By reducing the interface stiffness these actuators offer a better shock tolerance, a lower reflected inertia, more accurate and stable force control and less inadvertent damage to the environment.

2.2 ... to Variable Stiffness Actuators

However, the selected actuator stiffness typically optimizes this "power filtering" for only one single cadence. This limitation can be overcome with Variable Stiffness Actuators (VSA).

A VSA is a SEA in which the stiffness of the compliant element can be adapted. This allows, in the case of the application to lower limb prostheses, to tune the stiffness to adapt the prosthesis to the user but also to different gaits and tasks (e.g. climbing stairs).

On example of the implementation of a VSA in the application of biomedical robotics is the VSA developed by Bichi et al. [25].

There are also other contributions in this field, which all do have an advantageous compliant behaviour, but in order to change the compliance and obtain different control actions, energy has to be supplied. It is important, for a viable solution in prosthetic applications, that changing the actuator stiffness should requires little to no energy. In theory, this would be possible if the

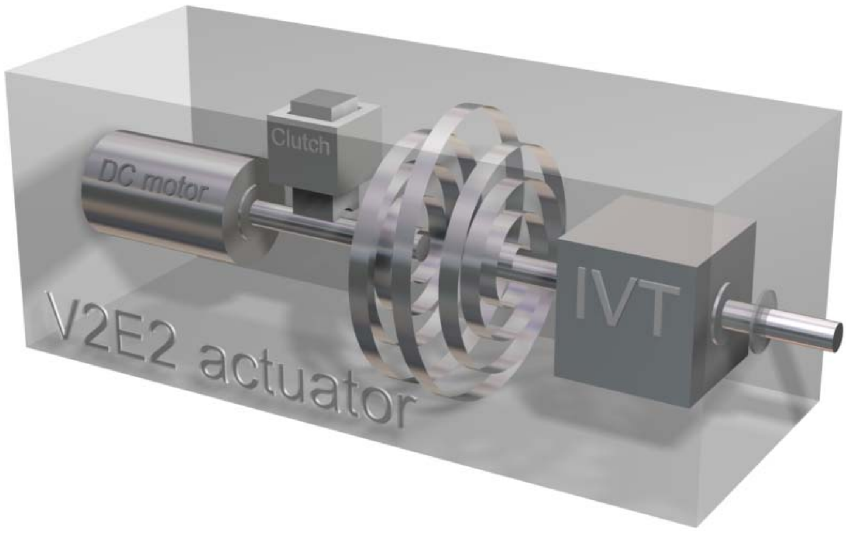

Figure 2.1: Conceptual sketch of the V2E2 actuator. From Stramigioli et al. [22].

stiffness of the elastic element is changed, while in parallel, its equilibrium position is changed, such that the energy stored in the elastic element is kept constant.

This is why Stramigioli et al. [22] developed the Very Versatile Energy Efficient (V2E2) actuator. An actuator able to intelligently generate reusable energy whenever negative work is done, and able to use this energy whenever necessary. This actuator is a series combination of a standard actuator, an elastic element and an Infinitely Variable Transmission. A Conceptual sketch of this mechanism is shown in Figure 2.1. If this concept is applied to an ankle prosthesis, the main motor would just have to provide the mean positive power required at the ankle — i.e. the net positive energy provided during a walking cycle, divided by the cycle duration — while the stiffness would be constantly adapted to render the desired torque. This concept was validated in Everarts et al. [12]

2.3 A VSA in an active transfemoral lower limb prosthesis

Taking this concept to the application of 2 degree of freedom (DOF) transfemoral ankle-knee prostheses adds even more value to it. Indeed, combining the mechanism with a differential and an IVT at both joints would allow to harvest energy from both joints and to return this stored energy in different proportions to the two joints. A diagram illustrating this concept is shown in Figure 2.2.

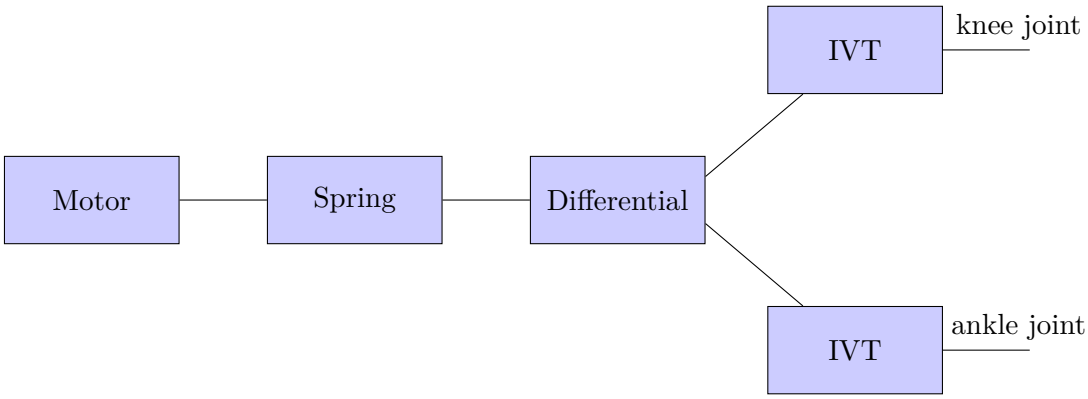

Figure 2.2: Diagram of the IVT based 2 DOF transfemoral ankle-knee prosthesis principle.

The combination of all these mechanical elements may seem heavy, and it is indeed heavier than presently available active transfemoral ankle-knee prostheses. But this is only considering the mechanism itself, in reality the weight of the battery supplying the prostheses also needs to be taken into account. Taking this also into account, as the IVT based prosthesis needs less energy per step, from a certain amount of steps on, the solution becomes advantageous.

This concept will be the main subject of the present work. A model is used to validate the concept and analyse its behaviour in closed-loop control. Adequate controllers are developed and the power flows in the prosthesis are extensively studied.

Chapter 3

CVT's and IVT's

3.1 Continuously Variable Transmissions

A Continuously Variable Transmission (CVT) is a transmission in which the transmission ratio can vary continuously, this in comparison with a gearbox transmission where there are no intermediate states between the different gears. The transmission ratio can vary continuously but is limited by the minimum and maximum admissible transmission ratios of the mechanism that define its operating range. The ratio of the transmission ratio extremes is called the ratio range. e.g.: if a CVT can vary its transmission ratio from 0.5 to 2, the ratio range is

$$rr_{CVT} = \frac{n_{CVT}|_{max}}{n_{CVT}|_{min}} = \frac{2}{0.5} = 4 \tag{3.1}$$

There are numerous applications for CVT's, amongst the most popular:

- Automotive applications: In conventional internal combustion engine cars, for every speed and needed propulsive force, a specific transmission ratio will yield the optimal fuel efficiency. This is why CVT's have been used in cars in replacement of the gearbox transmission. These CVT's have proved to improve the fuel savings and to reduce the vehicle emissions [8]. Another application is in automobiles using an energy storage flywheel. Here, due to the flywheel's inertia, the speed of the flywheel only changes slowly? A CVT is thus necessary to enable any desired output velocity [5].

- Flywheel presses are another typical example where energy is stored in the flywheel and released only at some instances.

In all these applications CVT's exist in various forms, here some of the CVT types are listed:

- V-belt CVT's are probably the most popular form of CVT's. In this kind of CVT a V-shaped belt connects two V-shaped pulleys to match the belt. The pulleys are made of two cones with summits facing. The cones can move to or away of each other changing the radius at which the V-belt matches the pulleys. The transmission ratio can then be calculated in as a function of both pulleys radii.

- Half toroidal CVT's are composed on the one hand of two facing cones which are incurvated in such a way that a torus could fit in between them. And on the other hand of one or more power rollers transmitting the power between the two disks (see Figure 3.1). The power rollers can turn around their axis but their axis can also turn around the center of the torus. This changes the contact points of the roller on the two disks, thus changing the transmission ratio. Full toroidal CVT's are the same as half toroidal CVT's except that the disks are larger continuing the curvature of the cones to form a full torus. In this type of CVT, their is no need for an external force on the power rollers because they are fully contained between the disks, this enhances the efficiency of the transmission.

- Cone CVT's are CVT's that use cones to make one or more gear radii vary. Some use belts to connect between two cones. Others, like the Turbo Trac Variator [9], use a disk

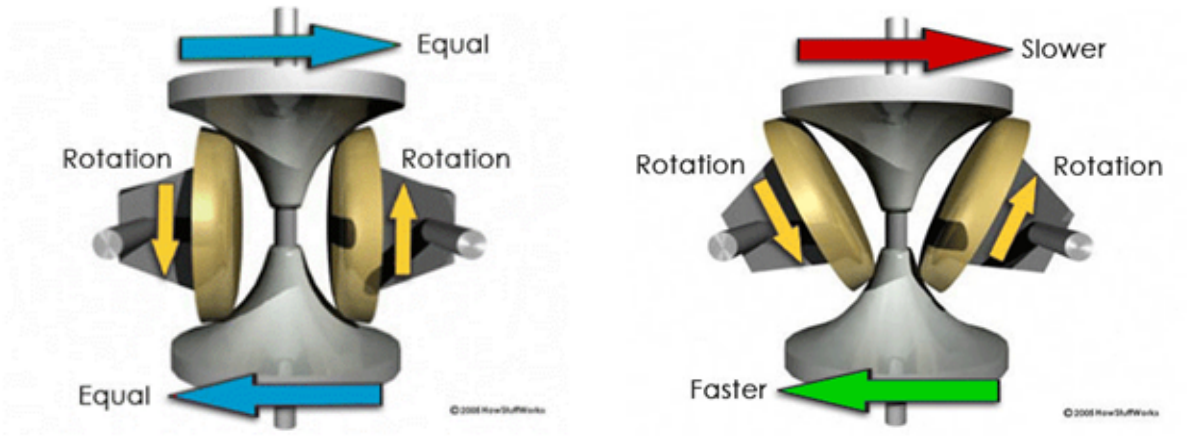

(a) *(b)*

Figure 3.1: Toroidal CVT. (a) the power rollers centred (b) the power rollers tilted. [Harris, William Howstuffworks "Toroidal CVTs"].

on an axis parallel to the cone's lateral surface that can move along its axis to make the contact point with the cone vary on the cone's lateral surface.

All these types of CVT's have one thing in common: The effective radius of one or more of the gears involved in the mechanism varies continuously. For it is not possible to find an integer number of teeth for each radius, cog-wheels are ruled out and thus this can only be achieved by friction.

3.2 Infinitely Variable Transmissions

An Infinitely Variable Transmission (IVT) is a CVT with an infinite ratio range, which means that the transmission ratio may achieve zero (i.e. an unmoving output shaft). Actually, some IVT's even achieve negative transmission ratios, reversing the output shaft rotation direction. This type of mechanism is generally constructed made up of three elements: a CVT, a planetary gear train (PG) (see Appendix B), and a fixed ratio mechanism (FR). These elements can be connected either in parallel or in series (see Figure 3.2). [18]

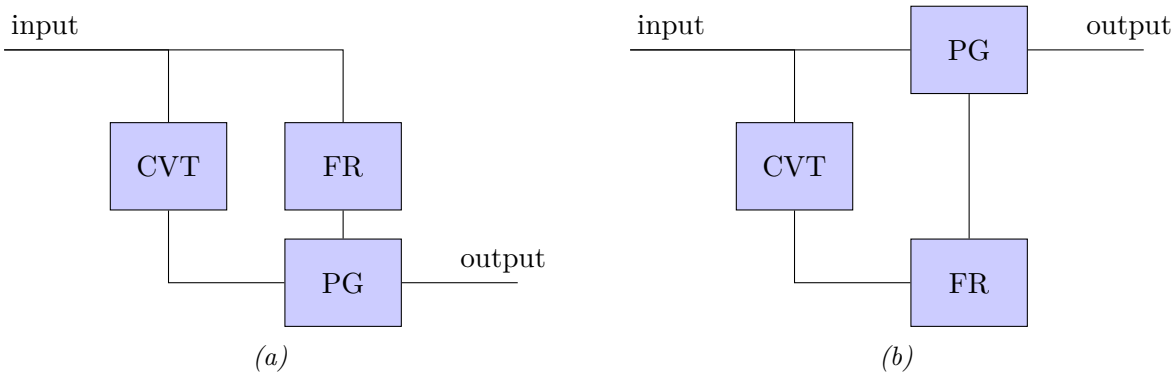

(a) *(b)*

Figure 3.2: (a) connections in a parallel IVT and (b) connections in a series IVT

3.3 The presently studied IVT

In the specific case of an IVT in a lower limb prosthesis the mechanism should be both compact and lightweight to fit in the prosthesis and not induce nuisance to the the amputees movements. The IVT should also be efficient, indeed if this is not the case the energy gained from storing mechanical energy is lost in the IVT and the main expected benefit of an IVT based prosthesis would be lost. In the mechanisms described in this chapter, due to friction, changing the ratio demands a considerable amount of energy and is almost impossible at rest. For the prosthesis application however, it would be desirable that the ratio can be changed at a lower cost and at rest.

Everarts et al. [13] developed a CVT that answers to these needs. The CVT is a planetary gear train whose planets are inclined and cone-shaped to induce a ratio variation by moving the contact point on the cone surface (see Figure 3.3a). For a better visualization it might be interesting to look at the CAD drawings of the actual prototype, these are provided in Appendix C (note that the colours of the CAD drawings correspond to the colors of Figure 3.3). The key feature is that the conical planets are inclined in such a way that their surface is tangent with a cylinder concentric with the annulus axis. This allows to move the annulus along its axis while keeping contact with the planets at all times. The input of this CVT is the planet carrier and, while the annulus is blocked in rotation, the output is the sun.

The annulus, or ring as it will we called hereafter in the context of the CVT, is composed of several rollers whose axes are perpendicular to the ring's axis (blocking all motion in the directions perpendicular to the ring's axis) and whose shape is such that they form a continuous circle at the inner side of the ring (see Figure 3.4). When moving the ring along its axis the rollers roll on the planets allowing to change the transmission ratio at minimal cost, and even when the CVT is at rest.

How the transmission ratio ($n_{CVT} = \frac{\omega_5}{\omega_8}$) depends on the position of the ring can be explained as follows:
As the CVT is a planetary gear train, the equation governing the ratio between the angular velocities of its different parts is (see Appendix B):

$$\frac{\omega_5 - \omega_8}{\omega_7 - \omega_8} = -\frac{R_{CVT,7}R_{CVT,6}}{R_{CVT,5}R'_{CVT,6}}, \tag{3.2}$$

with ω_i and $R_{CVT,i}$, respectively the angular velocity and the radius relative to the element labelled i in Figure 3.3. The rings velocity is zero, $\omega_7 = 0$, and the varying radius R'_6 can be expressed in terms of the position of the ring x (relative to the cone's apex) and the cone inclination angle α:

$$R'_6 = x \sin\alpha. \tag{3.3}$$

Equation (3.2) then becomes:

$$\frac{\omega_5 - \omega_8}{-\omega_8} = -\frac{R_{CVT,7}R_{CVT,6}}{R_{CVT,5}}\frac{1}{x \sin\alpha}. \tag{3.4}$$

Rearranging this equation to obtain the transmission ratio, $n_{CVT} = \frac{\omega_5}{\omega_8}$, gives:

$$n_{CVT} = \frac{\omega_5}{\omega_8} = 1 + \frac{R_{CVT,7}R_{CVT,6}}{R_{CVT,5}}\frac{1}{x \sin\alpha}. \tag{3.5}$$

For the application of the prosthesis the transmission needs to be an IVT whose ratio also sweeps over negative values. To turn the CVT in such an IVT, a planetary gear train is added as shown in figure Figure 3.3b. The output of the CVT, which was the sun of the first planetary gear is coupled to the sun of the added planetary gear. And the planet carrier of the CVT, is connected to the planet carrier of the added planetary gear, this represents the fixed ratio

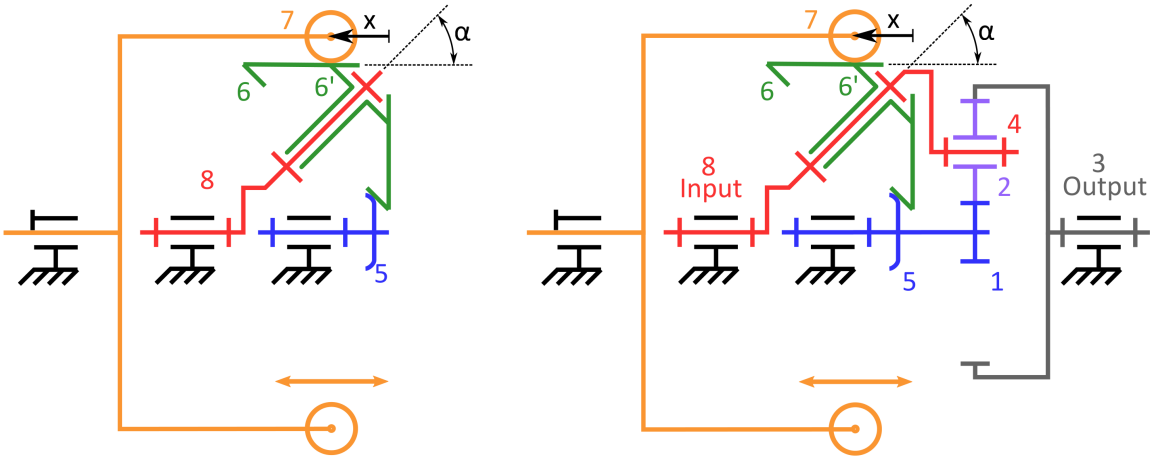

Figure 3.3: (a) Kinematic diagram of the CVT. In orange, the ring (that can be moved along its axis to change the transmission ratio); in red, the planet carrier (input); in green, the tilted planets; and in blue, the sun (output). (b) Kinematic diagram of the IVT. The parts that correspond to the CVT are in the same colors as in (a), the planet carrier is still the input. For the planetary gear: in blue, the sun; in purple, the planets; and in grey, the annulus (output). From Everarts et al. [13]

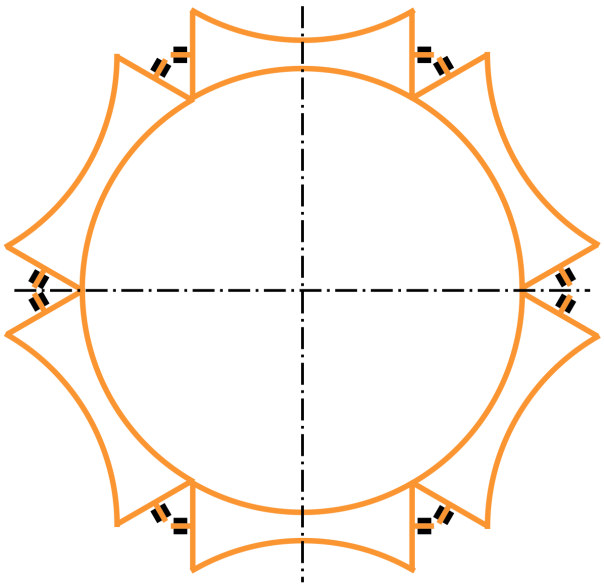

Figure 3.4: From Everarts et al. [13]The CVT ring composed of several rollers whose axes are perpendicular to the ring axis

mechanism of ratio 1. Indeed, since they are linked together, both planet carriers turn at the same speed. The annulus of the added planetary gear is now the output of the whole mechanism. This forms a parallel IVT as schematized in Figure 3.2a.

To derive the equation of the transmission ratio as a function of the ring position we start with the kinematic equation of the second planetary gear train (see Appendix B):

$$n_{PG} = \frac{\omega_1 - \omega_4}{\omega_3 - \omega_4} = -\frac{R_{PG,3}}{R_{PG,1}}, \tag{3.6}$$

with, again, ω_i and $R_{PG,i}$, respectively the angular velocity and the radius relative to the element labelled i in Figure 3.3. Introducing the kinematic constraints,

$$\omega_1 = \omega_5 \tag{3.7}$$

$$\omega_4 = \omega_8, \tag{3.8}$$

and combining equations (3.5) and (3.6) permits to derive the expression for the transmission ratio of the IVT as a function of the position of the ring:

$$n_{IVT} = \frac{\omega_3}{\omega_8} = 1 - \frac{R_{CVT,7}R_{CVT,6}R_{PG,1}}{R_{CVT,5}R_{PG,3}}\frac{1}{x\,\sin\alpha} \tag{3.9}$$

Looking at this equation it is appears that when

$$\frac{R_{CVT,7}R_{CVT,6}R_{PG,1}}{R_{CVT,5}R_{PG,3}}\frac{1}{x\,\sin\alpha} > 1$$

the IVT transmission ratio is negative.

A prototype of this IVT was built, the dimensions of the different parts of the CVT are:

$$\begin{cases} R_{CVT,5} = 10.9\,\text{mm} & (3.10) \\ R_{CVT,6} = 12\,\text{mm} & (3.11) \\ R_{CVT,7} = 30\,\text{mm} & (3.12) \\ \alpha = 45^\circ & (3.13) \\ x = [8;\ 21]\ \text{mm} & (3.14) \end{cases}$$

By adequately choosing the planetary gear radii $R_{PG,3}$ and $R_{PG,1}$ it is possible to obtain the desired ratio range.

Chapter 4

Modelling and control of the prosthesis

4.1 Model of the prosthesis

4.1.1 Introduction

As developed in Chapter 2, the prosthesis mechanism involves storing and releasing energy in a spring. On one side of the spring, the main motor provides the necessary energy by winding the spring. On the other side, the differential distributes the power to the two joints (knee and ankle) where we find the IVT's. These apply the necessary transmission ratios to provide the desired output torques. To study the behaviour of this mechanism — and in particular, the closed-loop behaviour of the mechanism — a model is needed.

Controlling the prosthesis in a torque control mode means providing the desired output torque at both joints at all times. This task can be divided into two subtasks:

1. controlling the main motor to sufficiently rewind the spring so that there is always enough energy stored in the spring to provide the necessary output power and;

2. controlling the IVT's to provide the joints with the desired output torque.

To fulfil the first task, the spring energy will be compared to a reference, being the input of the main motor controller. For the second task, a simplification is made. In the most realistic case, the model of the prosthesis should be connected to a model of the joint dynamics. The problem is that these dynamic systems are similar to inverted pendulums, and thus, are unstable. To circumvent this issue, we adopted a simplified framework where the kinematics of the joints are imposed. Joint kinematics systematically followed curves taken from the literature, whatever the torque being actually provided to the joints. The impact of this simplification will be discussed in Chapter 8. Transmission ratios, being necessary to deliver the required torques are thus also applied to the joint angular velocities. The resulting velocity — on the "input" side of the differential — will thus cause the spring to unwind (if both joints need to globally produce energy) or rewind (if both joints need to globally dissipate energy). Putting this all together, the model can be represented by the block diagram provided in Figure 4.1.

The following sections give a detailed description of the elements of the prosthesis and describe how they are modelled.

4.1.2 Main Motor

In a DC motor, the generated torque, T_m, is proportional to the armature current, I_m, by the motor's torque constant, K_m:

$$T_m = K_m I_m. \tag{4.1}$$

The armature circuit is a closed-loop circuit with, in series, the voltage applied to the motor, U_m, the armatures resistance, R_m, the armatures inductance, L_m and the back electromotive

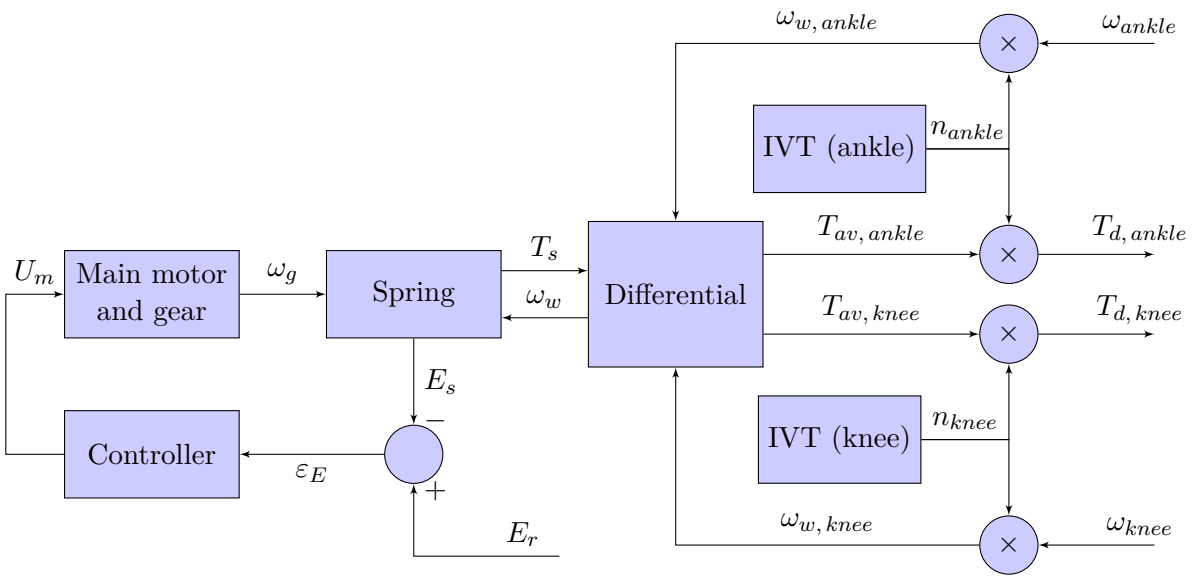

Figure 4.1: Block diagram showing how the prosthesis mechanism is modelled. Details about the symbols are available at the List of Symbols.

force (emf) induced by the motor's rotor. The back emf is proportional to the angular velocity of the shaft multiplied by the same torque constant:

$$\text{emf} = K_m \omega_m. \tag{4.2}$$

Based on Kirchoff's voltage law and Newton's second law of motion, it is possible to derive the equations describing the dynamics of a DC motor:

$$U_m = K_m \omega_m + R_m I_m + L_m \frac{\mathrm{d}I_m}{\mathrm{d}t} \tag{4.3}$$

$$J_m \frac{\mathrm{d}\omega_m}{\mathrm{d}t} = K_m I_m - B_m \omega_m - T_m. \tag{4.4}$$

The meaning of the different symbols is available at the List of Symbols. Neglecting the motor's inductance (i.e. assuming $L_m/R_m \ll J_m/B_m$), Equation (4.3) reduces to,

$$U_m = K_m \omega_m + R_m I_m. \tag{4.5}$$

The motor is connected in series with a gear (characterised by its gear ratio χ and its efficiency η_g) before it is connected to the spring:

$$\omega_g = \omega_m \frac{1}{\chi} \tag{4.6}$$

$$T_s = T_m \chi \eta_g. \tag{4.7}$$

Figure 4.2 shows how these equations are arranged in a block diagram.

4.1.3 Spring for mechanical energy storage

The spring is a torsional spring. The torque in such a spring depends on its stiffness, k, and its deformation angle from the equilibrium position. If the equilibrium position, $\theta_s = 0$, is chosen as reference for the spring angle, the torque in the spring is:

$$T_s = k\theta_s. \tag{4.8}$$

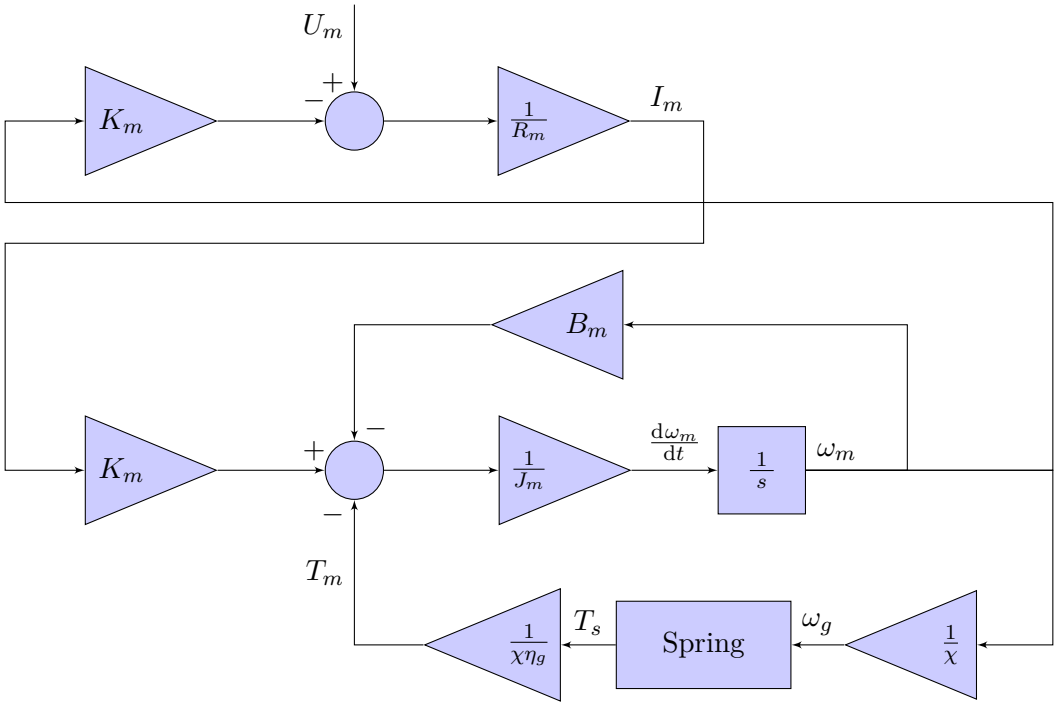

Figure 4.2: Main motor block diagram.

The energy stored in the spring depends on the square of the deformation angle:

$$E_s = \frac{k}{2}\theta_s^2. \tag{4.9}$$

The relative angular velocity of the spring, i.e. the difference between the velocities of its two connectors, will govern its loading/unloading behaviour. With, the motor gear on one side, ω_g, and, differential on the other side, ω_w, this yields:

$$\omega_s = \omega_g - \omega_w. \tag{4.10}$$

The spring is loaded with an initial deformation angle $\theta_s = \theta_{s,0}$, and the integral over time of its relative angular velocity yields the variation in spring deformation.

$$\theta_s = \theta_{s,0} + \int \omega_s \,\mathrm{d}t. \tag{4.11}$$

4.1.4 Differential

The differential is a planetary gear (for details about planetary gears and the equations governing their behaviour regarding torque and velocity please refer to Appendix B) where the planet carrier is the input and the annulus and sun the outputs. The output torques depend on the input torque and the gear ratios:

$$T_{an} = \frac{N_{an}}{N_{su} + N_{an}} T_{ca} \tag{4.12}$$

$$T_{su} = \frac{N_{su}}{N_{su} + N_{an}} T_{ca}. \tag{4.13}$$

Where T_{an}, T_{su} and T_{ca} are the torques at, respectively, the annulus, the sun and the carrier. And, N_{an} and N_{su} are the number of teeth of, respectively, the annulus and the sun.

In the case of the differential of the presently studied prosthesis, the output torque at the annulus is somewhat higher (18.18%[1]) than the torque at the sun. In parallel, in all tasks considered in this thesis (see Section 1.4), the highest torque peaks are exerted on the ankle joint. This is why the ankle joint is connected to the annulus and the knee joint to the sun. The torque proportions are thus:

$$T_a = \frac{N_{an}}{N_{su} + N_{an}} T_s \tag{4.14}$$

$$T_k = \frac{N_{su}}{N_{su} + N_{an}} T_s, \tag{4.15}$$

where T_a, T_k and T_s are the torques at, respectively the ankle joint, knee joint and spring side of the differential. At this stage,the differential efficiency is not taken into account.

The angular velocities of the ankle and knee joint after they have passed through the IVT's combine in the following way:
In a planetary gear, the ratio between the velocities of the sun and annulus relative to the carrier are equal to minus the ratio between the number of teeth in the annulus and the sun.

$$\frac{\omega_{su} - \omega_{ca}}{\omega_{an} - \omega_{ca}} = -\frac{N_{an}}{N_{su}}. \tag{4.16}$$

Since, the the carrier is connected to the spring and the annulus and sun to the ankle joint and knee joint respectively, Equation (4.16) rewrites.

$$\frac{\omega_{w,\,knee} - \omega_w}{\omega_{w,\,ankle} - \omega_w} = -\frac{N_{an}}{N_{su}}. \tag{4.17}$$

Finally rearranging Equation (4.17) leads to:

$$\omega_w = \frac{\frac{N_{an}}{N_{su}} \omega_{w,\,ankle} + \omega_{w,\,knee}}{1 + \frac{N_{an}}{N_{su}}}. \tag{4.18}$$

4.2 IVT planetary gears dimensioning

The range of gear ratios offered by the IVT's determines, for a certain torque being available at the IVT's input, the range of torques they can deliver. This range of gear ratios is determined by the CVT and the planetary gear the IVT is made of, and can be adjusted by changing the number of teeth of the sun and annulus of the planetary gear. Using equations (3.5), (3.6) and (3.9), the transmission ratio of the IVT can in fact be expressed in terms of the transmission ratio of the CVT and the gear ratio of the planetary gear:

$$n_{IVT} = 1 + n_{PG} \left(n_{CVT} - 1 \right). \tag{4.19}$$

Keeping in mind that the gear ratio of the planetary gear is negative; the maximum and minimum IVT transmission ratio are obtained for, respectively, the minimum and maximum values of the CVT transmission ratio:

$$n_{IVT}|_{\max} = 1 + n_{PG} \left(n_{CVT}|_{\min} - 1 \right) \tag{4.20}$$

$$n_{IVT}|_{\min} = 1 + n_{PG} \left(n_{CVT}|_{\max} - 1 \right). \tag{4.21}$$

[1] The difference in torque divided by the mean of the torques: $\frac{2\left(T_{an} - T_{su}\right)}{T_{an} + T_{su}} = \frac{2\left(N_{an} - N_{su}\right)}{N_{an} + N_{su}}$.

As the ankle joint and the knee joint have different torques operating ranges, the IVT's should be different as well. For each joint the maximum and minimum torque on all tasks considered in this work (see Section 1.4) are retained. Equalling the ratio between the maximum and minimum torque and the maximum and minimum IVT transmission ratio gives:

$$\frac{T_{max}}{T_{min}} = \frac{1 + n_{PG}\left(n_{CVT}|_{\min} - 1\right)}{1 + n_{PG}\left(n_{CVT}|_{\max} - 1\right)}. \tag{4.22}$$

Solving this equation for n_{PG} gives, respectively, for the ankle and the knee joint,

$$\begin{cases} n_{PG,\,ankle} = -0.4341 & (4.23) \\ n_{PG,\,knee} = -0.3395. & (4.24) \end{cases}$$

Possible values for number of teeth of the IVT planetary gears are given in Table 4.1 but other combinations are also possible.

Table 4.1: Number of teeth for the sun and the annulus for the planetary gears of the IVT's used for this model.

	N_{su}	N_{an}
ankle	48	111
knee	48	141

Note that the torque at the output of the IVT's is roughly a hundred times smaller than the torque needed at the joints. In the real prosthesis the mechanism that transmits the torque at the output of the IVT's to the joints will have to integrate a torque multiplication system. A possible solution is to work with a ball screw and a lever. Both these mechanisms have a very high efficiency, this is why, in this work, the torque at the output of the IVT's is multiplied by an ideal constant ratio. This justifies why Equation (4.22) suffices to dimension the IVT planetary gears.

4.3 Prosthesis control

4.3.1 Main motor control

The main motor input is the voltage delivered at its terminals. This motor's function is to reload the spring so that its energy fluctuates around a reference, E_r. This guarantees that the spring is able to provide the necessary power to the prosthesis joints. Concretely, when the spring energy is lower than the reference, the motor should provide more power. In contrast, if the spring energy is higher than the reference, the motor should provide less power. Consequently a simple proportional gain controller on the spring energy error is a good candidate for this controller.

However, if no voltage is applied to the motor, there can be no current and thus no torque being delivered. This means that the spring will unwind through the motor. Of course, this would immediately create an error on the desired spring energy which would result in a voltage to the motor again. In sum, there would always be an offset between the desired spring energy and the mean energy the spring fluctuates around. This is a classical illustration that a sole proportional controller cannot cancel a steady-state error. To solve this problem, we added a feed-forward component to the controller, i.e. a reference voltage U_r. We would chose this reference voltage so that the mean of the energy in the spring corresponds to the desired spring energy.

Figure 4.3 shows a block diagram for this controller.

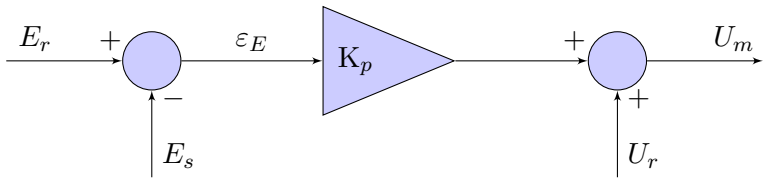

Figure 4.3: Controller for the main motor.

4.3.2 Computation of the IVT transmission ratios

As mentioned before, the prosthesis is torque controlled, meaning that the prosthesis should always provide the desired torques at its joints, as accurately as possible. Controlling these output torques is done through the control of the IVT transmission ratios.

To find the proper transmission ratios of the IVT's, the simplest solution is to compute the ratio between the desired torque, T_d, and the torque being currently available at the input of the IVT, T_{av}:

$$n = \frac{T_d}{T_{av}} \tag{4.25}$$

Assuming, of course, that the available torque at the IVT input is known. In practice torque sensors are very expensive and it is not likely that a commercial prosthesis would be equipped with these. Still it would be possible to determine the available torque by measuring the spring deformation (a cheaper solution) and computing the IVT input torque following the mechanical path to the IVT input.

The IVT transmission ratios can vary within a limited range of possible values. Said differently, the IVT transmission ratios are physically limited and thus the controller output should be saturated.

Figure 4.4 shows a block diagram for this controller.

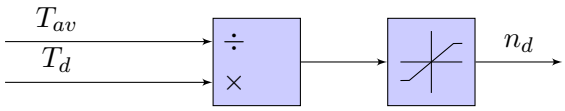

Figure 4.4: Controller to find the transmission ratios at the IVT's.

4.4 Experimental validation of the model and controllers

For the simulations in this section and all following simulations in this thesis, the simulations are solved with the ode45 integrator (a Matlab ODE solver based on the Dormand–Prince method, [11], [21]).

4.4.1 Spring parameters

In this case where no losses are considered at the level of the differential and the IVT's the total energy needed for the tasks of level ground walking and descending stairs is negative (more energy is stored in the spring than the spring has to produce). With power losses this is of course not realistic, this is why, at this stage, only the task of climbing stairs is analysed. The reference voltage, U_r, was set experimentally to coincide with the mean of the voltage that need to be applied to the motor for this task. The gain, K_p, of the proportional term of the controller was set so that the time response of the system is approximately the same as the duration of one step. The reference for energy in the spring is arbitrary set to an energy corresponding to 10 turns in the spring. The influence of these parameters will be analysed in Section 7.1 in order to make more discerning choices.

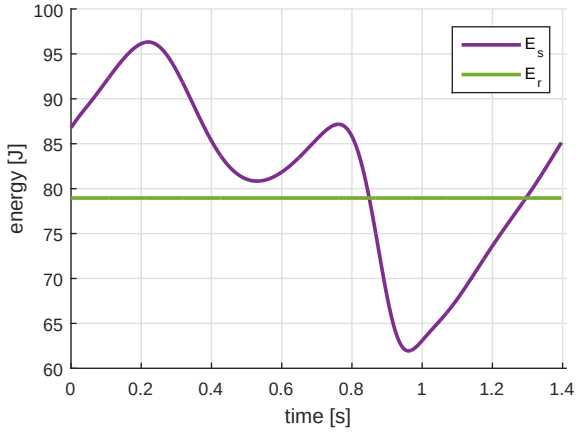

Figure 4.5: Spring energy for climbing stairs (purple) compared to reference (green).

Figure 4.5 shows that the spring energy stays around the reference energy. It is possible to deduce from this figure that there are to parts in the step where more energy in consumed, i.e. at the two instances where the energy decreases (these actually correspond to the powered knee extension and the powered plantar flexion). The first time the energy decreases it started of higher than the reference and thus the command to the motor stays below the mean voltage to the motor, U_r. The second time the energy decreases in the step it reaches below the reference, this results in a positive contribution of the proportional term of the main motor controller and thus the motor command gets higher than the mean voltage to the motor, U_r. This until the energy in the spring coincides with the reference again.

4.4.2 Torque tracking

Figures 4.6b and 4.6d show the transmission ratios that are computed with the transmission ratio controller described in Section 4.3.2. When looking at figures 4.6a and 4.6c it is clear that these transmission ratios care for a perfect tracking of the desired torque at the joints: the torque profiles at the joints and the desired torque profiles superimpose perfectly.

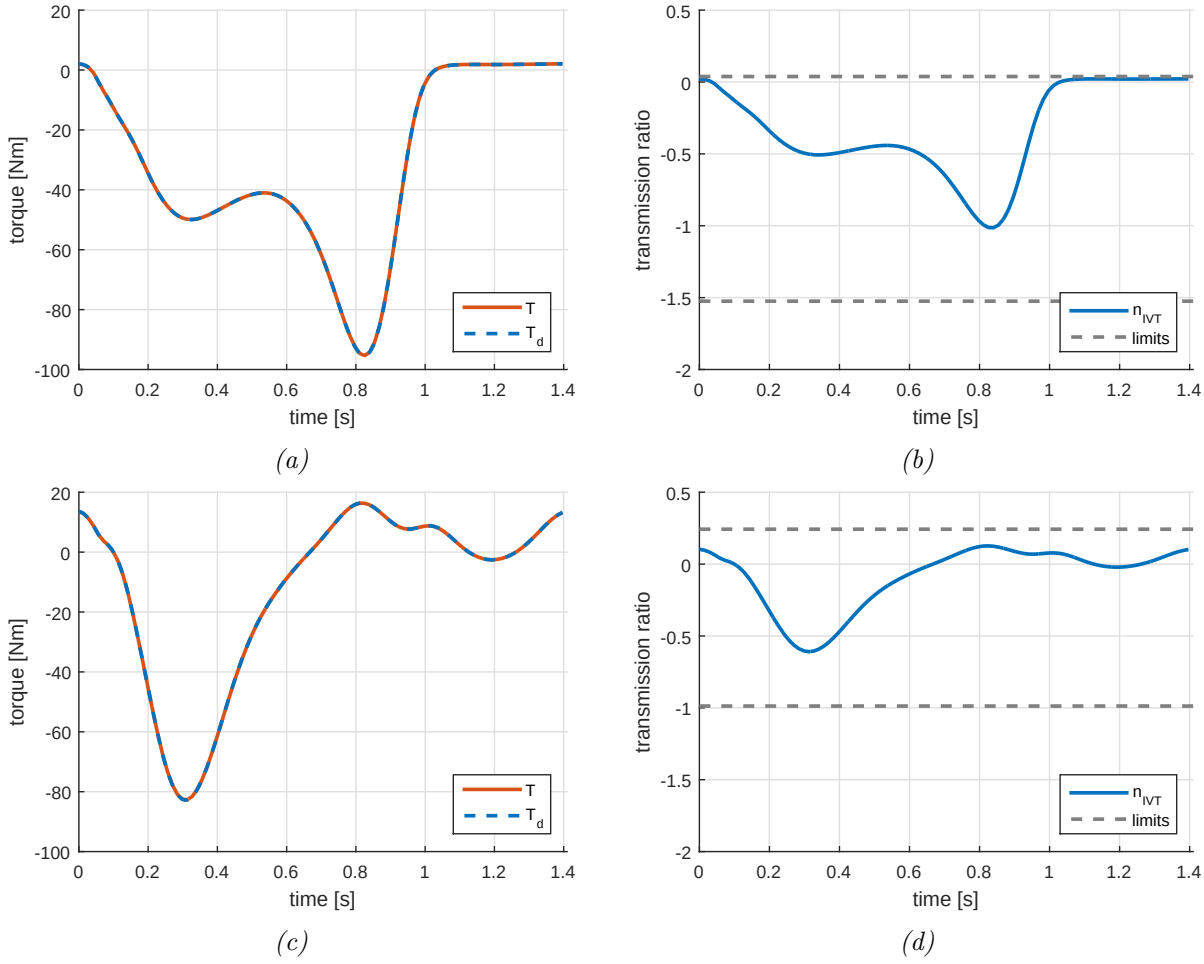

Figure 4.6: (a) and (c) Tracking of torque during the task of level ground walking at the joints. Blue is the desired torque; red the torque at the joint for, (a) the ankle joint, and (c), the knee joint. (b) and (d) IVT transmission ratios at the joints during the task of level ground walking for, (a), the IVT at the ankle joint, and (b), the IVT at the knee joint.

Chapter 5

Actual modelling of the IVT ratios control

The IVT transmission ratios multiply with the torques and angular velocities coming from the differential,

$$T_{ankle} = T_{av,\,ankle} n_{ankle} \qquad \omega_{w,\,ankle} = \omega_{ankle} n_{ankle} \tag{5.1}$$

$$T_{knee} = T_{av,\,knee} n_{knee} \qquad \omega_{w,\,knee} = \omega_{knee} n_{knee} \tag{5.2}$$

In the previous chapter, we assumed that these transmission ratios can vary instantaneously. In this chapter we introduce a model of the dynamics od the ratio control, i.e. captureing how the ratios depend on the positions of the rings of the CVT parts of the IVT's (see Equation (3.9)) and that that these rings are moved with a DC motor.

5.1 Model of the IVT motors

The positions of the rings of the CVT's are obtained by moving the rings with a DC motor and a lead screw. The lead screw transforms the rotational motion into linear motion with a coefficient k_{LS}: $x = k_{LS}\theta_i$ or $\frac{\mathrm{d}x}{\mathrm{d}t} = k_{LS}\omega_i$ or still $\frac{\mathrm{d}^2x}{\mathrm{d}t^2} = k_{LS}\frac{\mathrm{d}\omega_i}{\mathrm{d}t}$. In the case of the IVT motors, the motor must only provide torque when moving the CVT ring but not when the ring is at rest. The torque results from the acceleration of the ring:

$$T = \frac{k_{LS}}{\eta_{LS}} F = \frac{k_{LS}}{\eta_{LS}}\, m \frac{1}{\eta_r} \frac{\mathrm{d}^2x}{\mathrm{d}t^2} = \frac{k_{LS}^2}{\eta_{LS}\eta_r}\, m \frac{\mathrm{d}w}{\mathrm{d}t}. \tag{5.3}$$

η_{LS} and η_r capture the efficiency of, respectively, the lead screw and the CVT ring, which are not equal to 1 due to, respectively, the losses in the lead screw and friction in the ring. If this is added to the motor inertia, an equivalent inertia can be computed:

$$J_{eq} = J_i + \frac{k_{LS}^2 m}{\eta_{LS}\eta_r}. \tag{5.4}$$

The equations describing the dynamics of the IVT motors can be derived in the same way as for the main motor (see Section 4.1.2):

$$U_i = K_i\omega_i + R_i I_i \tag{5.5}$$

$$J_{eq}\frac{\mathrm{d}\omega_i}{\mathrm{d}t} = K_i I_i - B_i\omega_i. \tag{5.6}$$

The meaning of the different symbols is detailed in the List of Symbols. Again, the motor's inductance is neglected (i.e. assuming $L_i/R_i \ll J_i/B_i$). Figure 5.1 shows how these equations are arranged in a block diagram.

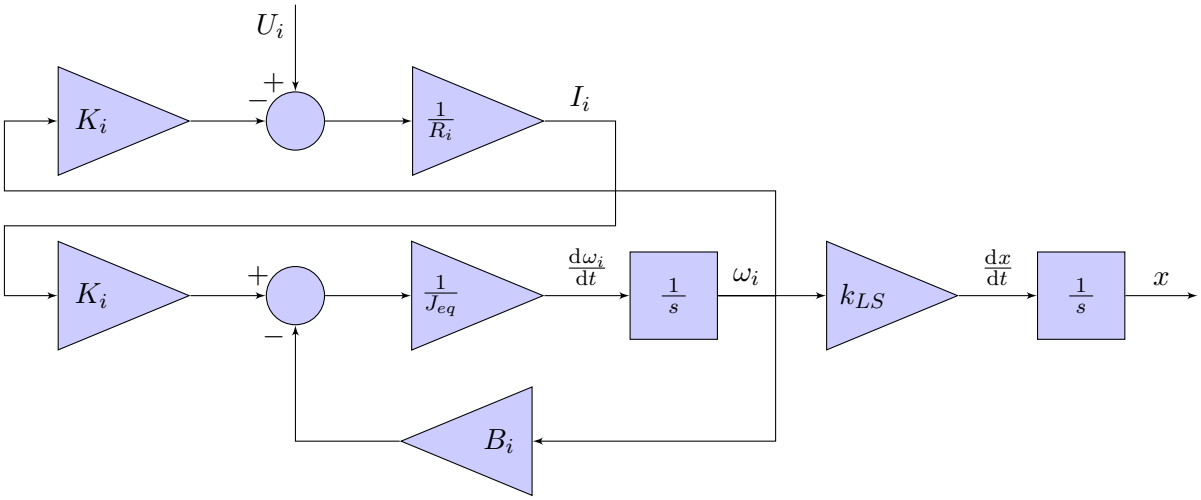

Figure 5.1: IVT motor block diagram.

5.2 IVT motors control

The first step in the control of the IVT motors, is to convert the desired transmission ratios into the positions of the rings of the IVT's corresponding to these transmission ratios. This is achieved by using Equation (3.9) that gives the transmission ratio as a function of the ring position of the IVT, x, and isolating x. Once the desired ring position is known, x_d, it is compared to the actual position of the ring, x, which yields an error, ε_x. This error is used as an input for the motor controller. The bigger the error, the faster the motor should move the ring to reach the desired position. A proportional-derivative controller is adequate for this task.

In particular, the derivative term is useful since it boosts the motor command when the error is increasing and reduces overshoot by predicting when the desired position is approached (i.e. when the error is decreasing). The input to the derivative term is filtered with a first order filter and a filtering coefficient N. This allows to filter out noise coming from the sensors. Of course, when using the model, the measuring of position is exact and there is no noise in the signal. However, in the model it will allow to filter out sudden error jumps due to quick changes in the desired positions. The transfer function of this filter is:

$$\frac{\mathrm{N}}{s+\mathrm{N}} = \frac{1}{\frac{1}{\mathrm{N}}s+1} \tag{5.7}$$

The higher N, the lower the time constant of the first order filter, the more high frequency fluctuations pass through the filter. At the opposite, if N is very small, the filter acts as an integral term with a very low gain and thus cancels the derivative term. This means a compromise needs to be found between filtering out the noise and keeping the effect of the derivative term.

A block diagram of this controller is presented in Figure 5.2.

5.3 Experimental validation of the IVT motors model and controller

5.3.1 IVT motors energy consumption

Simulations were run for the model with de model of the IVT motors added. The electrical power profiles of the IVT motors is given in Figure 5.3. The mean electrical powers for these motors are, respectively, for the ankle and the knee, 0.3 W and 0.1 W. This is much lower than the power consumed by the main motor.

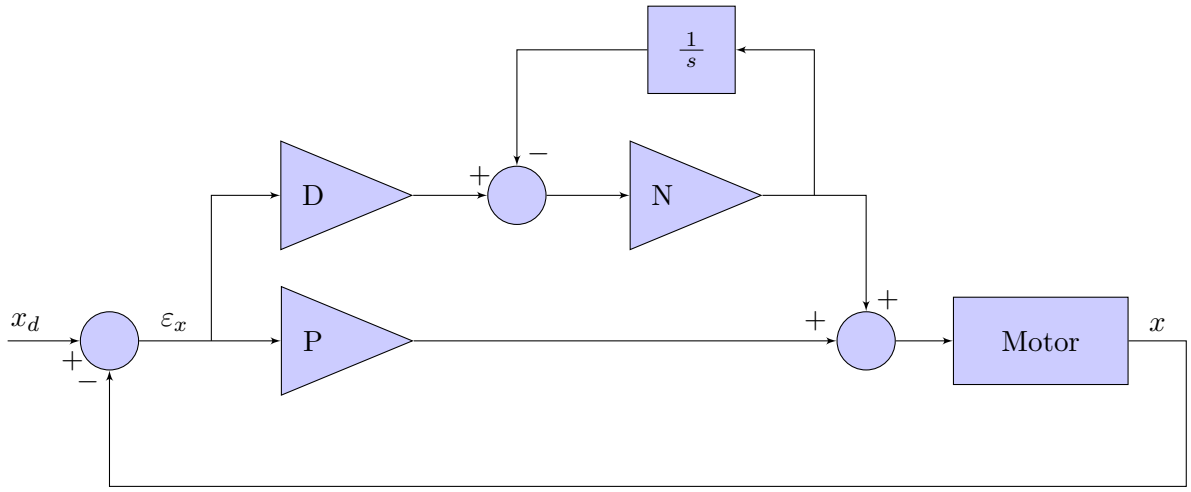

Figure 5.2: Controller for the IVT motors.

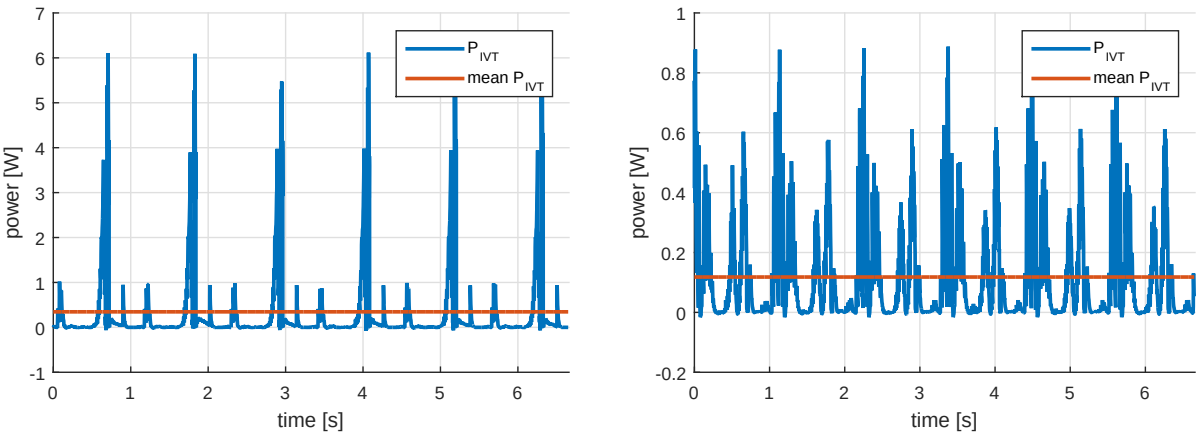

(a) *(b)*

Figure 5.3: Blue, the IVT motors power profiles, red, the mean IVT motor power. (a) IVT motor at the IVT at the ankle joint and (b) IVT motor at the IVT at the knee joint.

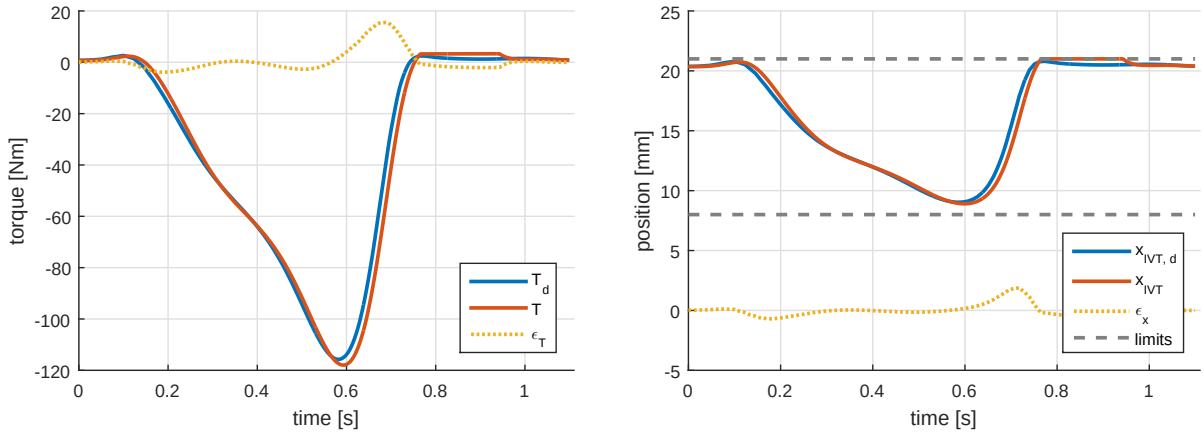

(a) *(b)*

Figure 5.4: (a) Tracking of torque during the task of level ground walking at the ankle. (b) position of the ring of the CVT of the IVT at the ankle during the task of level ground walking. For both graphs, blue is the signal to track; red is the tracking; and the dotted yellow line is the error.

5.3.2 Torque tracking

In Figure 5.4b it is possible to compare the actual position of the ring of the CVT of the IVT at the ankle joint with de desired one. The desired position corresponds to the position that would be needed to achieve the transmission ratios as computed in the previous chapter by the transmission ratio controller. The actual position of the ring fairly well fit the desired position, only at some places there is an error equal to 1 or 2 mm. The impact of this on the torque at the joints can be observed in Figure 5.4a. The torque tracking is not perfect any-more but still very acceptable.

Chapter 6

Mechanical energy dissipation in the prosthesis parts

Up to this chapter, the model captures power losses in the motors and within their gears or lead screws, but neither in the differential nor in the IVT's. However, both of these parts are based on gears, so that friction induces losses. Modelling these losses is furthermore more challenging than for the other parts. Indeed, power losses within the different parts of the mechanism occur in all possible power flow directions. And, in a prosthesis where energy is stored and released during the gait cycle, power flows are very important to consider. In the case of this prosthesis, the power flowing through the differential can go to, and come from, either the knee joint or the ankle joint, which makes the problem even harder.

6.1 Modelling the power losses

When power flows through a mechanical element, due to friction, some of this power is dissipated, and thus not transmitted to the output. These losses in torque translate to a lower power at the output of the mechanical element than at its input

$$P_{out} < P_{in}. \tag{6.1}$$

The ratio between these two quantities, defines the efficiency of the mechanical element

$$\eta = \frac{P_{out}}{P_{in}} < 1. \tag{6.2}$$

In the model, efficiency is applied as follows. When the power flows through a mechanical element from the spring, P_s, to the joints, P_{jnt}, i.e. when $P > 0$ (called direct power flow hereafter in this document), P_s is P_{in} and P_{jnt} is P_{out}. The relation between the power at the spring and joints sides of the mechanical element writes

$$P_{jnt} = \eta P_s. \tag{6.3}$$

This highlights that the spring has to produce more power than is actually needed at the joints. In contrast, when the power is flowing through a mechanical element from the joints, P_{jnt}, to the spring, P_s, i.e. when $P < 0$ (called inverse power flow hereafter in this document), P_{jnt} is P_{in} and P_s is P_{out}. The relation between the power at the spring and joints sides of the mechanical element now writes

$$P_{jnt} = \frac{1}{\eta} P_s. \tag{6.4}$$

In this case, the spring receives less power than the power dissipated by the joints. Such a situation would for instance happen when both joints need to dissipate mechanical energy, i.e. to break, for instance when descending stairs.

As explained in Section 4.1.1, the model does not directly use power as a variable but rather torque and angular velocity. The spring deformation angle is decreased or increased through

Table 6.1: Different possible scenarios regarding the sign of torque and angular velocity and the effect of power losses on each one of them. T_{spr} and T_{jnt} are the torques at, respectively, the spring side and the joint side of the elements that induce losses. ω_{spr} and ω_{jnt} are the angular velocities at, respectively, the spring side and the joint side of the IVT's. $n_{\eta=1}$ corresponds to the IVT transmission ratios if no losses are considered. The 'effect' column describes what the effect of the power losses is on the spring in comparison with the case were no losses are considered. θ_s is the deformation angle of the spring.

Power flow	Torque	Ang. velocity	Transmission ratio	effect
$P > 0$	$T_{spr} > T_{jnt} > 0$	$\omega_{jnt} > \omega_{spr} > 0$	$n > n_{\eta=1} > 0$	decreasing θ_s more ...
$P > 0$	$-T_{spr} < T_{jnt} < 0$	$\omega_{jnt} < \omega_{spr} < 0$	$n < n_{\eta=1} < 0$	decreasing θ_s more ...
$P < 0$	$T_{jnt} > T_{spr} > 0$	$\omega_{spr} < \omega_{jnt} < 0$	$n_{\eta=1} > n > 0$	increasing θ_s less ...
$P < 0$	$T_{jnt} < -T_{spr} < 0$	$\omega_{spr} > \omega_{jnt} > 0$	$n_{\eta=1} < n < 0$	increasing θ_s less ... ... than if the efficiency of the elements was equal to 1

the joint angular velocities. This will make the spring energy vary, so that the spring has to provide or harvest mechanical power.

Torque drops then appear at the various elements of the mechanism. In the case of direct power flow, this decreases the available torque at the joint. Conversely, in the case of inverse power flow, the torque at the joint side of the elements, T_{jnt}, is larger than the torque at the spring side, T_{spr}.

To understand how the drop in torque induces the need for power compensation (positive or negative), at the level of the spring, during unwinding and rewinding, it is necessary to have a closer look at the IVT transmission ratios.

In the case of direct power flow: Because of the drop in torque ($T_{jnt} < T_{spr}$), the IVT transmission ratios need to increase to provide the desired output torque. As these same transmission ratios apply to the joint angular velocities, the spring is unwound more than if the efficiencies of the elements was set to 1.

In the case of inverse power flow: Because of the drop in torque ($T_{spr} < T_{jnt}$), the IVT transmission ratios need to decrease to provide the desired output torque. As these same transmission ratios apply to the joint angular velocities, the spring is rewound less than if the efficiencies of the elements was set to 1.

For a better understanding of this very important phenomenon, the different scenarios are summarised in Table 6.1.

6.1.1 Power flows and losses in the differential

The differential is the node in the mechanism where three power flows come together: the power coming from, or going to, the spring, the ankle joint and the knee joint. These three power flows can all go in either directions and are added in a Kirchoff junction rule fashion. Two cases have however to be rejected: the power flows can neither all arrive in the differential (no place to store energy there) nor all depart from the differential (energy can not be produced by the differential). 6 ($= 2^3 - 2$) possibilities remain, in each case the energy losses need to be computed in the appropriate way, this is summarised in Table 6.2.

The configuration presented in Figure 6.1 shows how this is implemented in the model. It provides the correct efficiency relation in all 6 cases. The reader is encouraged to check consistency with the cases presented in Table 6.2 to better understand how this operates. This figure is interesting to state the problem. However, the "`if else`" clauses induce discontinuities which is source of issues for numerical solvers. This is why the clauses were replaced by a

Table 6.2: 6 different possible scenarios for power flows in the differential. P_s, P_a and P_k are the powers coming from or going to the spring, the ankle joint and the knee joint, respectively. The direction of the arrows indicate in which direction the power flows.

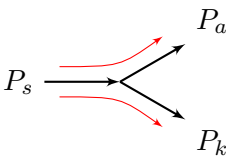 $P_a + P_k = \eta P_s$	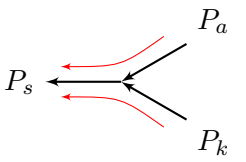 $P_s = \eta(P_a + P_k)$
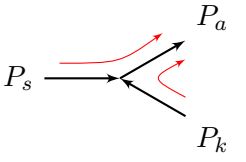 $P_a = \eta(P_s + P_k)$	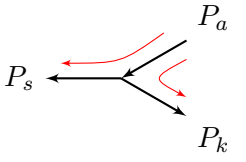 $P_s + P_k = \eta P_a$
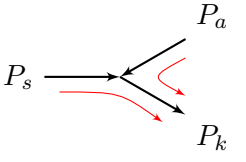 $P_k = \eta(P_s + P_a)$	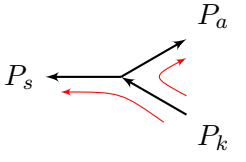 $P_s + P_a = \eta P_k$

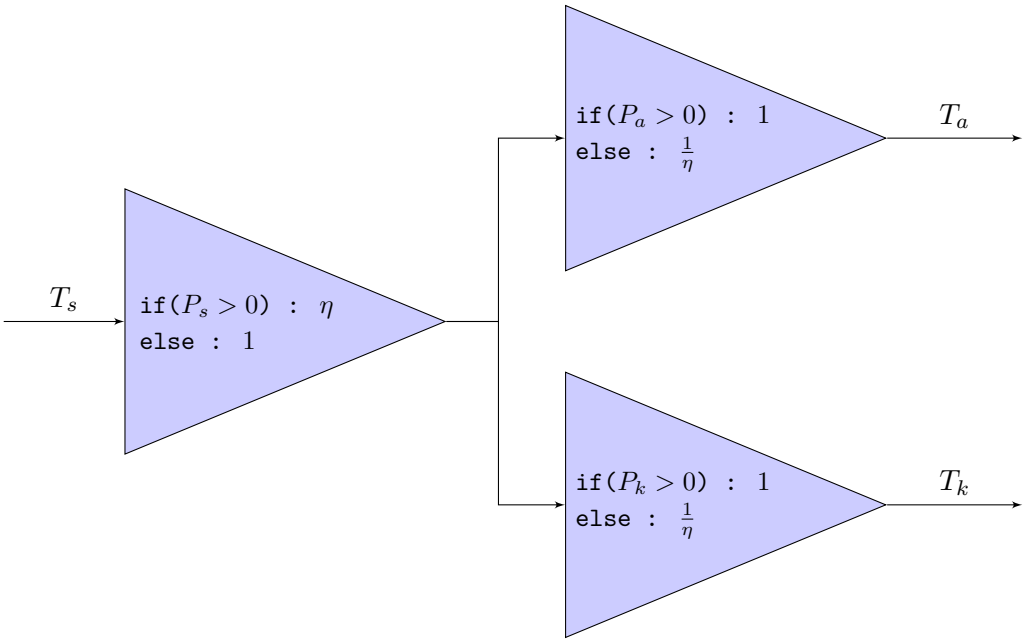

Figure 6.1: Implementation of the efficiency in the differential of the model. P_s, P_a and P_k are the powers coming from or going to the spring, the ankle joint and the knee joint respectively. Powers are considered positive when flowing from the spring to the joints and negative when flowing from the joints to the spring. T_s, T_a and T_k are the torques at, respectively, the spring, the ankle joint and the knee joint side of the differential. Note that here the differential gear ratios themselves are not represented.

sigmoid function, inducing smoother transitions between the different cases. The functions corresponding to, respectively, the left and the right blocs are:

$$f_1\left(\frac{P}{P_{max}}\right) = \eta + (1-\eta)\left(\frac{1}{2} - \frac{1}{\pi}\text{arctg}\left(a\frac{P}{P_{max}}\right)\right) \tag{6.5}$$

and

$$f_2\left(\frac{P}{P_{max}}\right) = 1 + \frac{1-\eta}{\eta}\left(\frac{1}{2} - \frac{1}{\pi}\text{arctg}\left(a\frac{P}{P_{max}}\right)\right) \tag{6.6}$$

where P is either P_s, P_a or P_k[1] according to the considered gain block. P_{max} is the maximum absolute value of the considered power along the power profile of all tasks considered in this work (see Section 1.4). a is a constant value that determines the steepness of the drop. A high a will make the change steeper. These functions are plotted in Figure 6.2a and Figure 6.2b respectively.

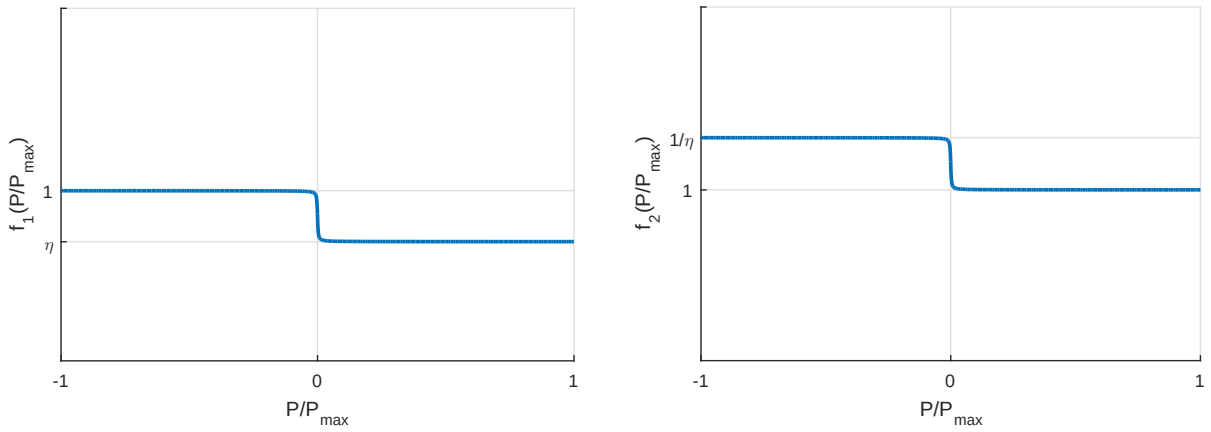

(a) *(b)*

Figure 6.2: (a) Quantity corresponding to Equation (6.5). (b) Quantity corresponding to Equation (6.6). For both quantities $a = 512$. The horizontal axis represents the normalised power (P/P_{max}).

6.1.2 Power flows and losses in the IVT's

For including the efficiency of the IVT's in the model, the principle is the same although there are only two possibilities. Either the power flows trough the IVT in one direction, or the other. Only one gain block suffices on the torque trajectory. If the power is positive, the gain is η, if the power is negative, the gain is $\frac{1}{\eta}$. Again a sigmoid function is used to avoid discontinuities,

$$f_3\left(\frac{P}{P_{max}}\right) = \eta + \frac{1-\eta^2}{\eta}\left(\frac{1}{2} - \frac{1}{\pi}\text{arctg}\left(a\frac{P}{P_{max}}\right)\right) \tag{6.7}$$

where P can be either P_a or P_k for the IVT at the ankle and knee joint respectively and P_{max} and a are the same as before. This function is plotted in Figure 6.3.

[1] same variables as in Table 6.2 and Figure 6.1

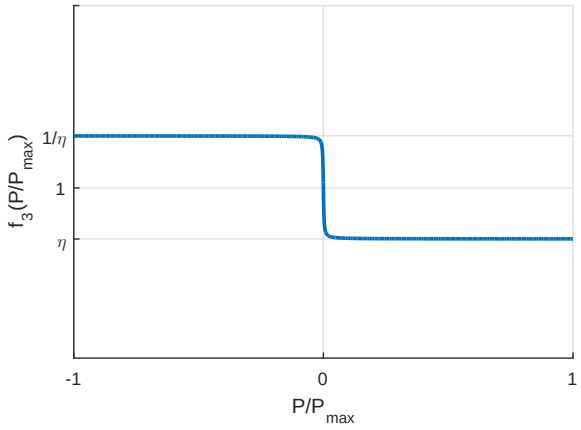

Figure 6.3: Quantity corresponding to Equation (6.7) for $a = 512$. The horizontal axis represents the normalised power (P/P_{max}).

In the case of the IVT there is another important aspect regarding power flows. The power does not flow directly from the input to the output but also circulates inside the the IVT. There are two possible power flow configurations in the IVT, they are shown in Figure 6.4.

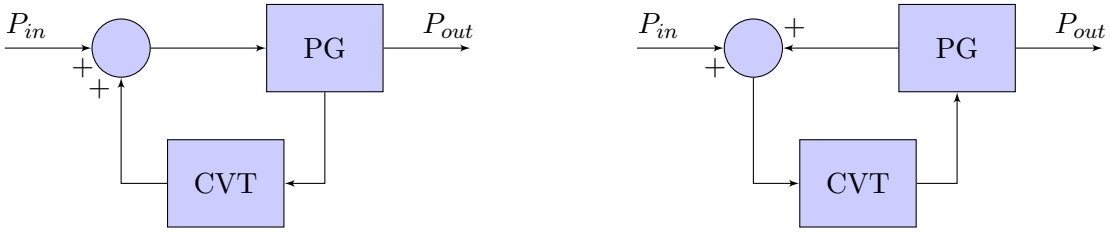

(a) Type I flow *(b) Type II flow*

Figure 6.4: Two possible power flow configurations in the IVT.

The more power circulates in the CVT branch, the more power is lost due to the losses in the CVT [30]. The amount of power circulating in the CVT branch depends on the overall transmission ratio of the IVT. If the efficiency of the CVT and the PG are known, the overall efficiency of the IVT can be calculated with the following two formulas, derived by Mangialardi and Mantriota [18]:

$$\text{Type I flow:} \qquad \eta_{IVT} = \frac{n_{IVT}\left(1 - \frac{\eta_{PG}}{n_{CVT}}\right)}{1 - \eta_{CVT}\eta_{PG} + n_{IVT}\left(\eta_{CVT} - \frac{1}{n_{CVT}}\right)} \tag{6.8}$$

$$\text{Type II flow:} \qquad \eta_{IVT} = \frac{\eta_{CVT} n_{IVT}\left(\frac{1}{n_{CVT}} - \eta_{PG}\right)}{1 - \eta_{CVT}\eta_{PG} + n_{IVT}\left(\frac{\eta_{CVT}}{n_{CVT}} - 1\right)}. \tag{6.9}$$

The efficiencies of the CVT and the planetary gear can be approximated to, respectively, $\eta_{CVT} = 0.85$ and $\eta_{PG} = 0.98$. Using equations (6.8) and (6.9) overall efficiencies of the IVT's are obtained in function of their transmission ratio. The results are plotted in Figure 6.5.

It is clear that the mean efficiency is significantly lowered compared to the efficiency of the CVT. However, the poorest efficiencies occur at the lowest transmission ratio values (in absolute value). This is good new because, if the transmission ratio is small, the torque losses are also small. For the value of the efficiency of the IVT that will be used for this project it would thus

be more appropriate to use a weighted mean, weighted in function of the transmission ratio. The weighted means for both IVT's are:

$$\begin{cases} \eta_{IVT,\,ankle} = 0.6557 & (6.10) \\ \eta_{IVT,\,knee} = 0.5875 & (6.11) \end{cases}$$

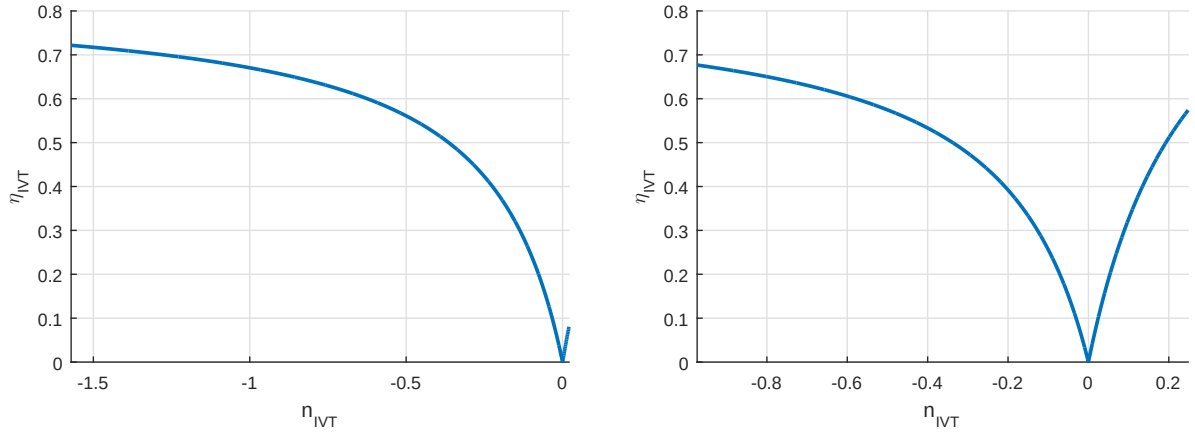

(a) *(b)*

Figure 6.5: Efficiency of the IVT's in funcion of their transmission ratio. (a) the IVT at the ankle, (b) the IVT at the knee.

6.2 Revisiting the dimensioning of the IVT planetary gears

As explained above, introducing power losses in the model decreases the available torque at some instances. The IVT transmission ratios then need to go beyond the previously computed limits. The range of the IVT's should thus be updated.

This is done by computing for each joint the maximum and minimum torque on all tasks considered in this work. But this time the torque profiles are first divided by the efficiency gains described in sections 6.1.1 and 6.1.2. This has as effect to take the torque drops into account and gives different values for T_{min} and T_{max}. Solving Equation (4.22), derived in Section 4.2, for n_{PG} gives the following new values:

$$\begin{cases} n_{PG,\,ankle} = -0.4387 & (6.12) \\ n_{PG,\,knee} = -0.3392. & (6.13) \end{cases}$$

Possible values for number of teeth of the IVT planetary gears are given in Table 6.3 but other combinations are also possible.

Table 6.3: Number of teeth for the sun and annulus of the planetary gears of the IVT's used for this model.

	N_{su}	N_{an}
ankle	48	109
knee	48	142

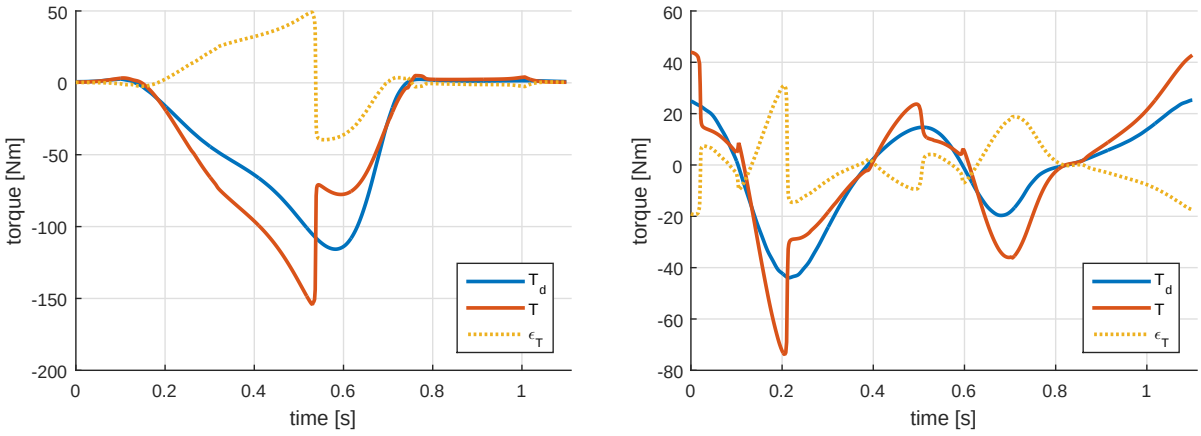

(a) *(b)*

Figure 6.6: Torque tracking with no integral term at the IVT gear ratio controllers in the case with all power losses considered. (a) torque tracking at the ankle joint; (b), torque tracking at the knee joint. For both graphs, blue is the desired torque; red, the torque at the prosthesis joint, and; yellow, the error.

6.3 Revisiting the transmission ratio controller

6.3.1 Adding an integral term

Now that the efficiency of the IVT's has been added to the model, the tracking of torque is not right any-more. Indeed, the controller compares the available torque at the input of the IVT's with the desired torque at their output but does not take efficiency into account. This efficiency decreases or increases the available torque, unbeknownst to the controller, resulting in an offset in the tracking of torque (see Figure 6.6). The only instances where a correct torque tracking is achieved is when the desired torque is zero.

The suggested solution is to add an integral term to the controller. The input of the integral term is the error between the joint output torque and the desired torque one. This integral term thus compensates for the torque loss due to the IVT limited efficiency. Furthermore, it also compensates a change in efficiency when the power flow changes direction. Note that this would not have worked out if the transmission ratio was multiplied by a constant compensation coefficient.

6.3.2 Adding an anti-windup system

Introducing a integral term in the controller brings another problem in. The IVT transmission ratios can vary within a limited range of possible values. Said differently, the IVT transmission ratios are physically limited and thus the controller output should be saturated. Control theory informs that such an output saturation with an integral term in the controller can easily lead to a wind-up error. To illustrate this, the IVT's were virtually brought to saturation. This was done by reducing the ratio at the joint after the IVT (see end of section Section 4.2). Figure 6.7a shows a windup error in the tracking of torque (around $t = 0.75\,\mathrm{s}$). Because of the interfering effect of the saturation, it is difficult to identify when not compared to a case with no wind-up error, but will become clear when compared just below.

To overcome this problem, an anti-wind-up system has to be added to the controller. In this case, this was implemented via back-calculation. It computes the difference between the output before and after a virtual saturation and subtracts the difference to the integral term before integration. This cancels the integral terms when the output is out of its physical limits;

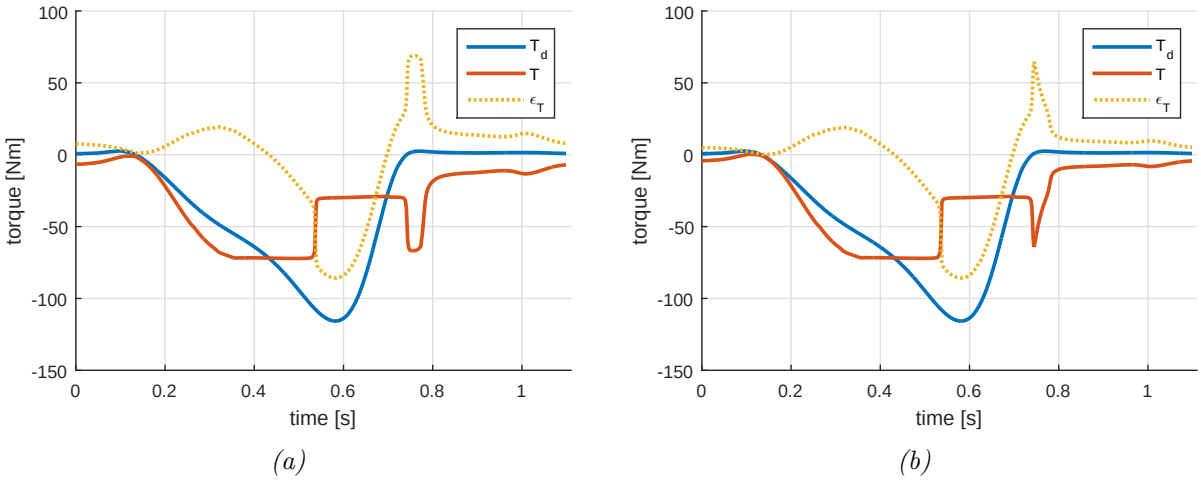

Figure 6.7: Comparison of torque tracking during the task of level ground walking at the ankle. Ror the IVT gear ratio controller with (a) and without (b) anti-windup system, in a case of saturation. For both graphs, blue is the signal to track; red is the tracking; and the dotted yellow line is the error.

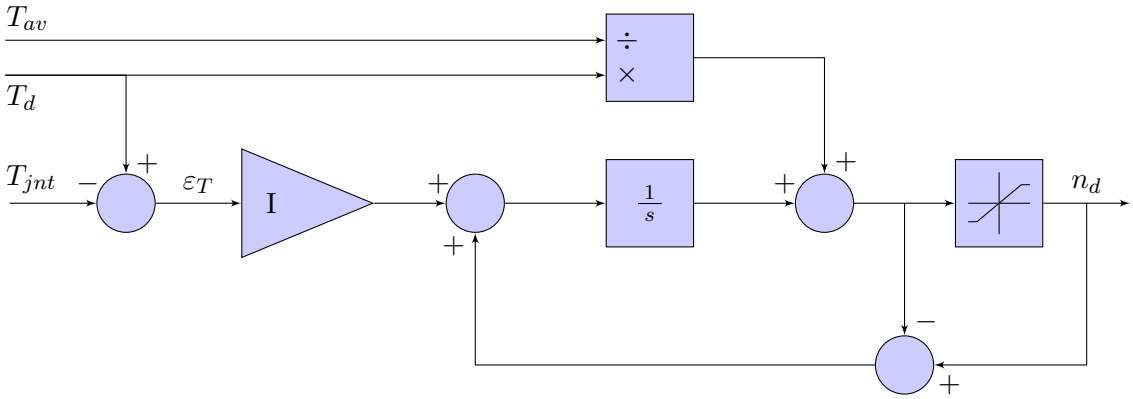

Figure 6.8: Updated controller to find the transmission ratios that the IVT's should provide.

and thus prevents wind-up errors. As soon as the signal is not saturated any-more, the back-calculation term goes to zero again and the effect of the integral term is restored.

Figure 6.8 presents a block diagram for the updated controller.

The same simulation with the virtual saturation was ran, but this time with the anti-windup system added to the controller. In Figure 6.7b the transmission ratio leaves saturation sooner (around $t = 0.75\,\mathrm{s}$) reducing the error on the tracking of torque.

6.4 Experimental validation of the model and updated controller

Figure 6.9a shows that with the new controller the offset in the torque tracking (see Figure 6.6) is corrected. The torque at the joint matches the desired torque relatively well except at one instant. At that instant, due to a reversal of the power flow, the available torque at the IVT drops (the cause of this drop will be explained more extensively in Section 7.2.1). The integral term of the IVT transmission ratio controller then cares to correct the static error induced by this torque drop , bringing the torque at the joint back on the profile of the desired torque. This is clear when looking at the graph of the desired position of the ring of the CVT of the IVT (see

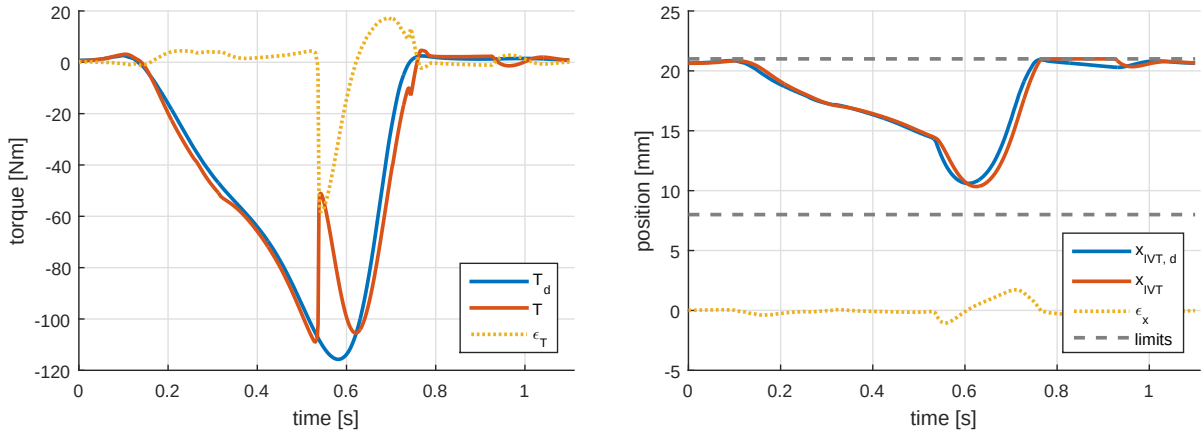

(a) *(b)*

Figure 6.9: (a) Tracking of torque during the task of level ground walking at the ankle. (b) position of the CVT ring of the IVT at the ankle during the task of level ground walking. For both graphs, blue is the signal to track; red is the tracking; and the dotted yellow line is the error.

Figure 6.9b). At the instant of the torque drop there is a discontinuity, suddenly increasing the desired position to increase the transmission ratio (in absolute value). A similar torque drop occurs around $t = 0.75\,\mathrm{s}$ but this one is much smaller because the absolute value of the torque itself is much smaller at that time.

Chapter 7

Energy consumption minimization and results

7.1 Energy consumption minimization

7.1.1 Dimensioning of the optimal main motor gear ratio

The main motor is connected in series with the spring through the motor gear. The gear ratio determines the rate at which the motor will operate. In a DC motor, there are two kinds of power losses.

1. Losses due to Joule heating, the production of heat as a consequence of current passing through the motor's wires. These losses are proportional to the motor's resistance and to the square of the current circulating in the motor. As the current is directly proportional to the torque in the motor; the higher the torque, the more power is lost through Joule heating.

2. Losses due to friction. These losses are proportional to the angular velocity of the motor's shaft. And thus, the higher the angular velocity, the more power is lost through friction.

Angular velocity and torque in the motor are linked proportionally through the speed torque gradient, C_m. The higher the torque, the lower the angular velocity and conversely. To limit the overall losses, a compromise has thus to be found between a low torque (lower losses due to Joule heating) and a low angular velocity (lower losses due to friction). Properly choosing this gear ratio is thus critical. It depends on the mechanical power the motor has to produce and on the torque in the spring.

In a real prosthesis, it would be difficult to change this gear ratio for the different tasks exposed in Section 1.4. It is more practical that only one reduction ratio does the job for all the tasks. It is however difficult to estimate in which proportion the prosthesis will be submitted to the different tasks. Consequently, we decided to optimise the gear ratio for the task of level ground walking. This task is likely the most predominant one.

Lets suppose for a moment that the motor is operating at constant rate. It is possible to compute the optimal motor rate, for a desired mechanical output power (this would be the mean power for flat walking in this instance), as follows:

- The efficiency of a motor is the ratio between the mechanical power ($\omega_m T_m$) it produces and the electrical power (UI) it is fed with. Here the torque at the output of the motor T_m is equal to the total torque in the motor (T) minus the friction torque in the motor ($B_m \omega_m$).

- The angular velocity of the motor depends on the motor voltage (U_m) multiplied by the speed constant less the torque (T) multiplied by the speed torque gradient (C_m). The speed constant is the inverse of the torque constant (K_m).

- The current in the motor can be derived from the torque (T) and the torque constant (K_m).

- The optimal rate for the motor is the rate at which the efficiency is at its maximum, or equivalently, where de derivative of the efficiency is zero.

This gives the system of equations:

$$\begin{cases} \eta = \dfrac{\omega_m \left(T - B_m \omega_m\right)}{U_m I_m} & (7.1) \\ \omega_m = \dfrac{U_m}{K_m} - C_m T & (7.2) \\ I_m = \dfrac{T}{K_m} & (7.3) \\ \frac{\partial \eta}{\partial T} = 0. & (7.4) \end{cases}$$

From these four equations, it is possible to derive the optimal torque and angular velocity for a certain voltage,

$$\begin{cases} T_{opt} = \dfrac{U_{m,\,opt}}{K_m} \sqrt{\dfrac{B_m}{B_m C_m^2 + C}} & (7.5) \\ \omega_{m,\,opt} = \dfrac{U_{m,\,opt}}{K_m} - C_m T_{opt}. & (7.6) \end{cases}$$

Finally, by computing the mechanical power, P_m, that is needed at the output of the motor,

$$P_m = \omega_m \left(T - B_m \omega_m\right), \tag{7.7}$$

and by substituting Equation (7.5) and Equation (7.6) in this last equation, it is possible to find the optimal voltage at which the motor should operate. This gives a first value for $U_{m,\,opt}$, T_{opt} and $\omega_{m,\,opt}$.

The mechanical power that is needed at the output of the motor is the sum of the powers needed at both joints, taking efficiency into account. The average of this value is the power the motor should deliver if it was delivering power at a constant rate. Using the data from the literature for level ground walking and considering the efficiency of the different elements of the mechanism, we found that the mean mechanical output power of the motor should be 20.74 W.

From this result it is possible to compute the optimal values, they are:

$$\begin{cases} U_{m,\,opt} = 16.5\,\mathrm{V} & (7.8) \\ \omega_{m,\,opt} = 604\,\mathrm{rad/s} & (7.9) \\ T_{m,\,opt} = T_{opt} - B_m \omega_{m,\,opt} = 31.4\,\mathrm{mNm}. & (7.10) \end{cases}$$

In reality, the motor is not operating at a constant rate and the mean efficiency is lower than in the case of the constant rate. The motor will drain a higher electrical power. It becomes very complicated to mathematically compute the optimal values. This is why a new value for $U_{m,\,opt}$ is experimentally determined. If $U_{m,\,opt}$ is too low, due to the motor's proportional controller, the mean voltage to the motor will be higher than this value and the motor gear will not be optimised. The same happens if the value for $U_{m,\,opt}$ is too high. With a dichotomous method, the value $U_{m,\,opt}$ was tuned to match the mean voltage for the task of level ground walking. The new optimal values are:

$$\begin{cases} U_{m,\,opt} = 21.5\,\mathrm{V} & (7.11) \\ \omega_{m,\,opt} = 786\,\mathrm{rad/s} & (7.12) \\ T_{m,\,opt} = 40.8\,\mathrm{mNm}. & (7.13) \end{cases}$$

Using Equation (4.7), the value for $T_{m,\,opt}$ can be used to calculate the appropriate gear ratio for the main motor gear:

$$\chi = \frac{\overline{T_s}}{\eta_g T_{m,\,opt}}, \tag{7.14}$$

where $\overline{T_s}$ is the mean torque in the spring (derived from the reference energy).

7.1.2 Synthesis of the optimal main motor controller parameters

In this section, the influence of two parameters in three different tasks (level ground walking, climbing stairs and descending stairs) is discussed in order to select proper values for them minimizing energy consumption and offering a safe and stable behaviour of the prosthesis. These two parameters are:

1. the spring reference energy, E_r; and,
2. the main motor controller proportional term gain, hereafter K_p.

Level ground walking

The spring reference energy determines how much energy should be stored in the spring. The higher this energy (E_r) is, the less significant the energy needed to complete a single cycle from a task with the prosthesis (e.g. one step on flat ground) is towards it. But, on the other hand, the higher the energy, the higher the torque in the spring. On the motor side of the spring, this is not a problem because we can adapt the motor gear ratio through Equation (7.14). On the other side however, it is important that the torque in the spring does not get higher than the maximal value allowed in the IVT's. The spring reference energy will be characterised by the number of turns in the spring N_s. Equation (4.9) can be rewritten:

$$E_r = \frac{k}{2}(2\pi N_s)^2 \tag{7.15}$$

To determine which energy levels will be studied, the following reasoning was followed:
The IVT's of this prosthesis can transmit torque up to a maximal torque capacity beyond which the IVT would get damaged. From this maximum torque allowed in the IVT's, it possible to compute the maximum torque that is allowed in the spring. By combining equations (4.8) and (4.14) we find that the maximum number of turns allowed is 12 turns. (To see what happens beyond, a case with 13 turns will also be studied.) To find the minimum number of turns, intuitively, we considered that the spring should contain at least the energy for two steps. This allows for, if something goes wrong, to have some backup energy left in the spring (e.g. the amputee sneezes, loses balance, and needs to perform two quick steps to recover and regain a stable position). This yields a minimum number of turns of 7:

$$2\overline{P_s}\Delta t_{step} = \frac{k}{2}(2\pi N_s)^2 \tag{7.16}$$

$$\left\lceil \frac{\sqrt{\frac{4\overline{P_s}\Delta t_{step}}{k}}}{2\pi} \right\rceil = {}^{1}N_s = 7. \tag{7.17}$$

with $\overline{P_s}$ representing the mean power the spring has to deliver during the task and Δt_{step} the duration of a step. Seven different energy levels will thus be studied corresponding to the spring loaded with 7 to 13 turns.

Running simulations for these different reference energies informs us that the influence of the energy in the spring has little impact on the the mean power of the main motor. For each reference energy level an optimal motor gear ratio, χ, is computed (see Equation (7.14)).

[1] the negative solution is of course rejected

Table 7.1: 6 different values for K_p analysed for level ground walking and corresponding response times for the system.

		×5	×2	÷2	÷5	
K_p [V/J]	15	3	1.5	0.75	0.15	0
Response time [s]	0.1	0.5	1	2	10	∞
		÷5	÷2	×2	×5	

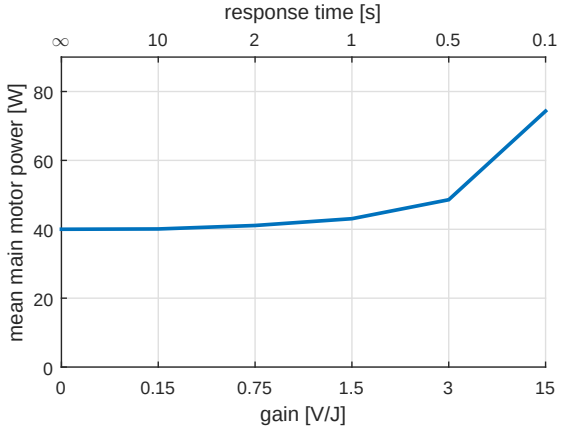

Figure 7.1: Mean main motor electrical power for level ground walking for different values of K_p. The top x-axis indicates the corresponding response times of the system. N_s is set to 10 (the median value of previously investigated energy levels). The horizontal axis is not a continuous scale.

The results also show that the energy in the spring has no big impact on the energy consumption of the IVT motors neither. This can be explained by the fact that the IVT motors consume most energy when sudden changes appear in the motors velocity. This occurs at rapid fluctuations in torque, just as it is the case in the rough profiles of the desired torque at the joints. It is true that, the lower the spring energy, the more the torque in the spring variates during the execution of the tasks. But the profile of variation of the torque in the spring is much smoother than the variation in the desired torque at the joints and has thus a negligible impact on the IVT motors energy consumption.

To study the impact of K_p, a good value to start with is a gain corresponding to a time response for the system of one second. This is of the same order of magnitude as the duration of a step. We then look what happens if we decrease or increase this gain or what happens when the gain is set to zero. 6 different gains will be analysed, they are covered Table 7.1.

In Figure 7.1, we see that the impact of K_p on the main motor energy consumption is much bigger than for the reference energy level. The higher the gain, the more energy the main motor consumes. This is in accordance with the fact that, the higher K_p, the more the input voltage of the motor fluctuates and the higher its peaks reach (see Figure 7.2). Still with the purpose of minimizing energy consumption of the prosthesis, this leads to chose the smallest possible value for K_p. In the next section will be explained why this value can not be set to zero.

As for the level of energy in the spring, the results revealed that K_p has little impact on the IVT motors energy consumption. It is true that the higher the gain, the more the energy in the spring stays close to the reference value. But for the same reasons as before, the impact of this is negligible compared to the effect of the rough fluctuations in the desired torque at the joints.

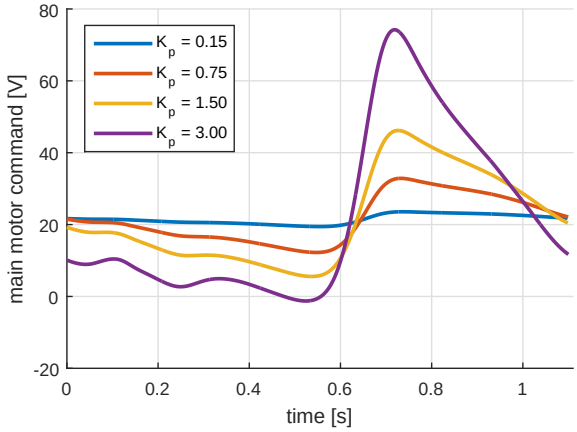

Figure 7.2: Motor command during one stride of level ground walking for different values of K_p *(units are* V/J*).* N_s *is set to 10 (the median value of previously investigated energy levels).*

Climbing stairs

In the task of climbing stairs the importance of K_p becomes more clear. Indeed, the reference voltage for the motor command was set based on the the mean power for the task of level ground walking. For climbing stairs, more power is required, and thus, the spring is unloaded more. This means that if the voltage to the motor does not rise in time to reload the spring enough, the spring will completely unwind and the system will collapse. Actually it is possible to check the minimum required value for K_p for each energy level such that the spring never runs out of energy. And even better, that the spring energy stays above a certain security level. An interesting value for this security level is the energy required for one step. This allows, if something goes wrong (e.g. the amputee misses a step) and the subject loses balance, to make a step to catch up. A stable region can now be identified, it is shown in Figure 7.3.

This figure shows that, to lower the value for K_p as much as possible, the energy in the spring should be as high as possible. The combination of parameters that result from this analysis is:

$$\begin{cases} N_s = 12 & (7.18) \\ E_{ref} = 114\,\text{J} & (7.19) \\ K_p = 1.5\,\text{V/J} & (7.20) \end{cases}$$

Results from the simulations for the task of climbing stairs allow to confirm that, the conclusions on the influence of the parameters for level ground walking, remain valid for the task of climbing stairs. The energy consumption of the main motor in function of the energy in the spring is constant, if not slightly descending. For increasing values of K_p the main motor energy consumption goes up (see Figure 7.4). The impact of the parameters on the energy consumption of the IVT motors is negligible.

Descending stairs

For the task of descending stairs, more energy is stored in the spring than the spring has to provide and thus the main motor has to dissipate energy. This is why this task does not come into consideration for the choice of the two parameters.

Concerning the IVT motors, the simulation results again confirm that the parameters have little impact on their energy consumption.

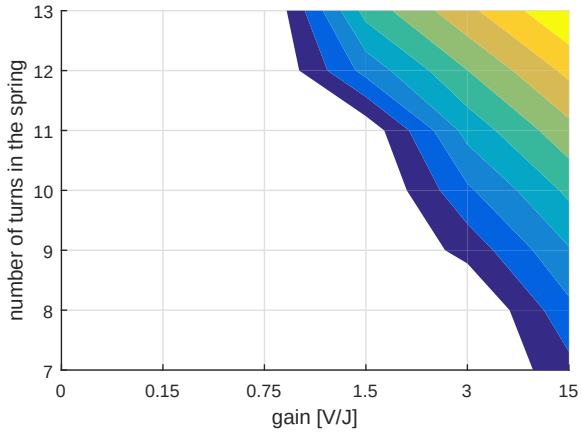

Figure 7.3: The coloured region represents the stable region for combinations of the parameters K_p *and* N_s *(i.e. the region for which the spring energy does not get lower than the energy required for one step when climbing stairs). The horizontal axis is not a continuous scale. The colors represent different energy levels above which the energy in the spring stays. Increasing linearly from blue, the energy needed for one step, to yellow, the energy needed for 8.3 steps.*

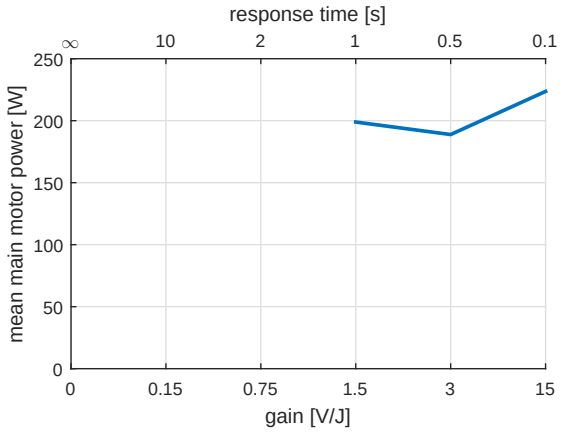

Figure 7.4: The mean main motor electrical power for climbing stairs for different values of K_p*. The top x-axis indicates the corresponding response times of the system.* N_s *is set to 12 (see Equation (7.18)). Missing values correspond to not stable combinations of* K_p *and* N_s*. The horizontal axis is not a continuous scale.*

7.2 Simulation results

In the previous section the parameters K_p and N_s were set through the analysis of simulation results. This section proposes a more detailed analysis of the results of the simulations for the three different tasks with the parameters set to the values found in the previous section. Two additional cases are studied:

1. the transition between level ground walking and climbing stairs, and;
2. the transition between level ground walking and descending stairs.

7.2.1 Level ground walking

Figure 7.5 shows the results of a simulation for level ground walking. On Figure 7.5a the spring energy fluctuates around the set reference energy. The angular velocity is positive most of the time, which means the spring is being rewound. Around 0.55 s the angular velocity drops in a negative peak that corresponds to the powered plantar flexion during the push-off phase. At the same time a corresponding decrease in energy is observed in the spring. The graph in Figure 7.5b shows the the electrical power feeding the motor and the power delivered by the spring as well as the powers needed at the ankle and knee joint. When the power at the joints is negative, the power at the spring is negative as well, meaning the spring is being rewound. At the power peak at the ankle, the knee joint brings in a small portion of the power, the rest is provided by the spring. Even so, the power peak in the spring is higher than the one at the ankle joint because power losses occur at the differential and at the IVT. At that time the motor receives more electrical power to reload the spring more to compensate the decrease in energy due to the big power peak.

The torque graphs (see Figure 7.5c and Figure 7.5e) show a reasonable tracking of the desired torque except at some particular instances as for example in the middle of the big torque peak at the ankle. At those instances torque drops occur and then the integral term of the gear ratio controller adapts the gear ratio to get back to the desired torque. This is very clear at the discontinuity in the graph of the position of the IVT ring at the ankle joint at time $t \approx 0.53$ s (see Figure 7.5d). The reason these torque jumps occur is because a reversal in the power flow direction inverses the efficiency relation between the power at the joint side and at the spring side of the mechanical elements, as in Equation (6.3) and Equation (6.4). The bigger the torque peak, the bigger the jump.

In particular in the case of the big torque drop at the ankle joint: before the torque drop, during the phase of controlled dorsiflexion, the power flows from the joints to the spring. The torque at the joint side of the mechanical elements is thus higher than the torque at the spring side. At the instant of the switch to the powered plantar flexion phase, the power flows from the spring to the joints and the torque at the joint side of the mechanical elements is now lower than at the spring side. The absolute value of the gear ratio increases to compensate for this drop in torque. As this happens in the middle of a big torque peak, this torque drop is relatively big compared to others that happen at the knee joint or in other tasks.

It is interesting to note that at these torque jumps, the IVT motors have to move the ring very fast to compensate. The energy consumption of IVT motors is thus highly correlated with number and amplitude of these torque jumps along the torque profile.

7.2.2 Climbing stairs

Figure 7.6 shows the results of the simulation for climbing stairs. The graph of the spring measurements in Figure 7.6a shows how the the spring energy first goes down to a new mean value around which it stabilises around. This has as effect to increase the motor command to reload the spring with more power than in the case of level ground walking. Which is in

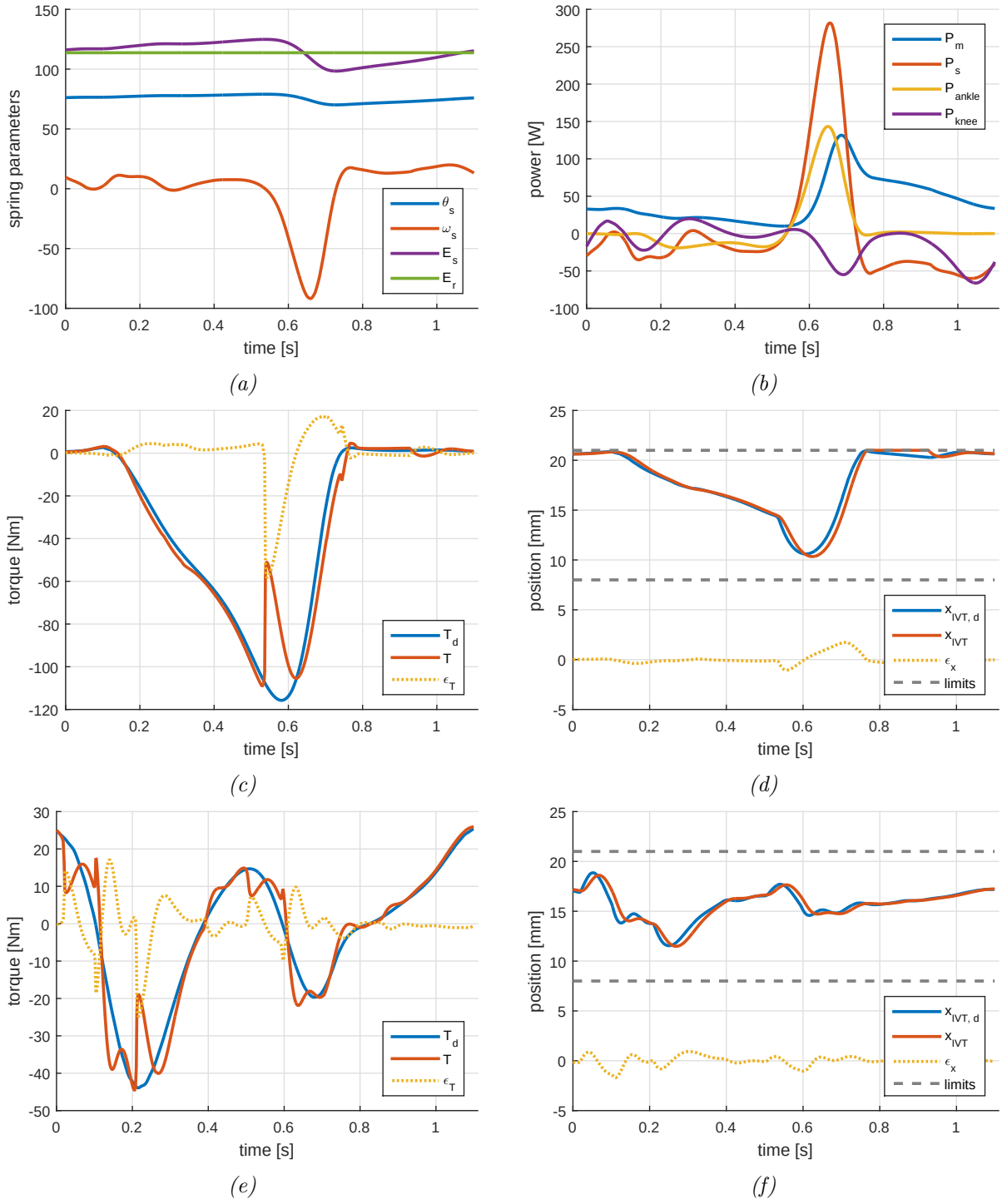

Figure 7.5: Simulation results for level ground walking. (a) the spring measures: blue, the spring deformation angle (in rad*); red, the spring deformation angular velocity (in* rad/s*); green and purple, the spring reference energy and the spring energy (in* J*). (b) powers at different stages of the mechanism (in* W*): blue, the electrical power to feed the main motor; red, the power delivered by the spring; yellow and purple, respectively, the powers required at the ankle and the knee joint. For graphs (c) through (f), blue is the signal to track, red is the tracking, and the dotted yellow line is the error. (c) is the torque developed at the ankle joint and, (d), the position of the CVT ring in the IVT at the ankle. (e) and (f) are the same for the knee joint.*

accordance with the fact that climbing stairs is a more energy consuming task than level ground walking. The system finds a new stable state after approximatively three steps.

In this task, smaller torque jumps are observed. There is one clear torque drop in the ankle torque profile (see Figure 7.6b) but as the torque at that moment is only about 50 Nm the jump is still smaller than the one in the torque profile for flat walking (which appears at a torque of about 120 Nm). Again, we can see the discontinuity in the position profile of the CVT ring of the IVT (see Figure 7.6c). At the knee joint there is a big torque peak but, as the power flow does not change direction during that peak, no torque jumps are observed there.

7.2.3 Descending stairs

Figure 7.7 shows the results of the simulation for descending stairs. In this case, the opposite happens than in the case of climbing stairs. The mean energy in the spring establishes at a value higher than the reference energy. This is the consequence of a task that produces more energy than it consumes. The stable state is reached even faster than in the case of climbing stairs.

There is one big torque drop in the torque profile of the ankle with corresponding discontinuity in the position profile of the CVT ring of the IVT (see Figure 7.7b and Figure 7.7c). At the knee joint there are some fluctuations in the torque and position of the ring around time $t = 0.4\,\mathrm{s}$ (see Figure 7.7d and Figure 7.7e), the repercussion of the fluctuations of the gear ratio in the spring angular deformation velocity is very clear (see Figure 7.7a).

7.2.4 From level-ground walking to climbing stairs

In Section 7.2.1 and Section 7.2.2 we studied the behaviour of the prosthesis in the tasks of level ground walking and climbing stairs separately. In reality, the amputee will go from one task to another, it thus interesting to study the transition between these tasks. Artificial data was created by making a junction between the end of the torque profile for level ground walking and the end of the torque profile for climbing stairs. this was also repeated for the torque at the knee joint and for the position profiles of both joints. Special attention was paid to keep the profiles synchronised after the transition, if this was not the case, it could highly affect the power profiles. The artificial transition was then put between one step of flat ground walking and three steps of climbing stairs (for observing stabilisation).

The results (see Figure 7.8) show a progressive decrease in the spring energy and increase in the electrical power feeding the motor. The system establishes around the same steady state as in the case of the separate task. The tracking of torque shows no different behaviour from the separate cases. Note that, as the artificial data was created using interpolations of the existing data, the minimum and maximum torque for this transition task stays within the same limits as the three separate tasks studied before.

7.2.5 From level-ground walking to descending stairs

For the transition from level ground walking to descending stairs artificial data was created in the same way as for the transition to climbing stairs. Here again, the spring energy progressively increases to oscillate around the steady state of the separate task of descending stairs. There are no problems observed in terms of tracking torque at the transition between the two tasks.

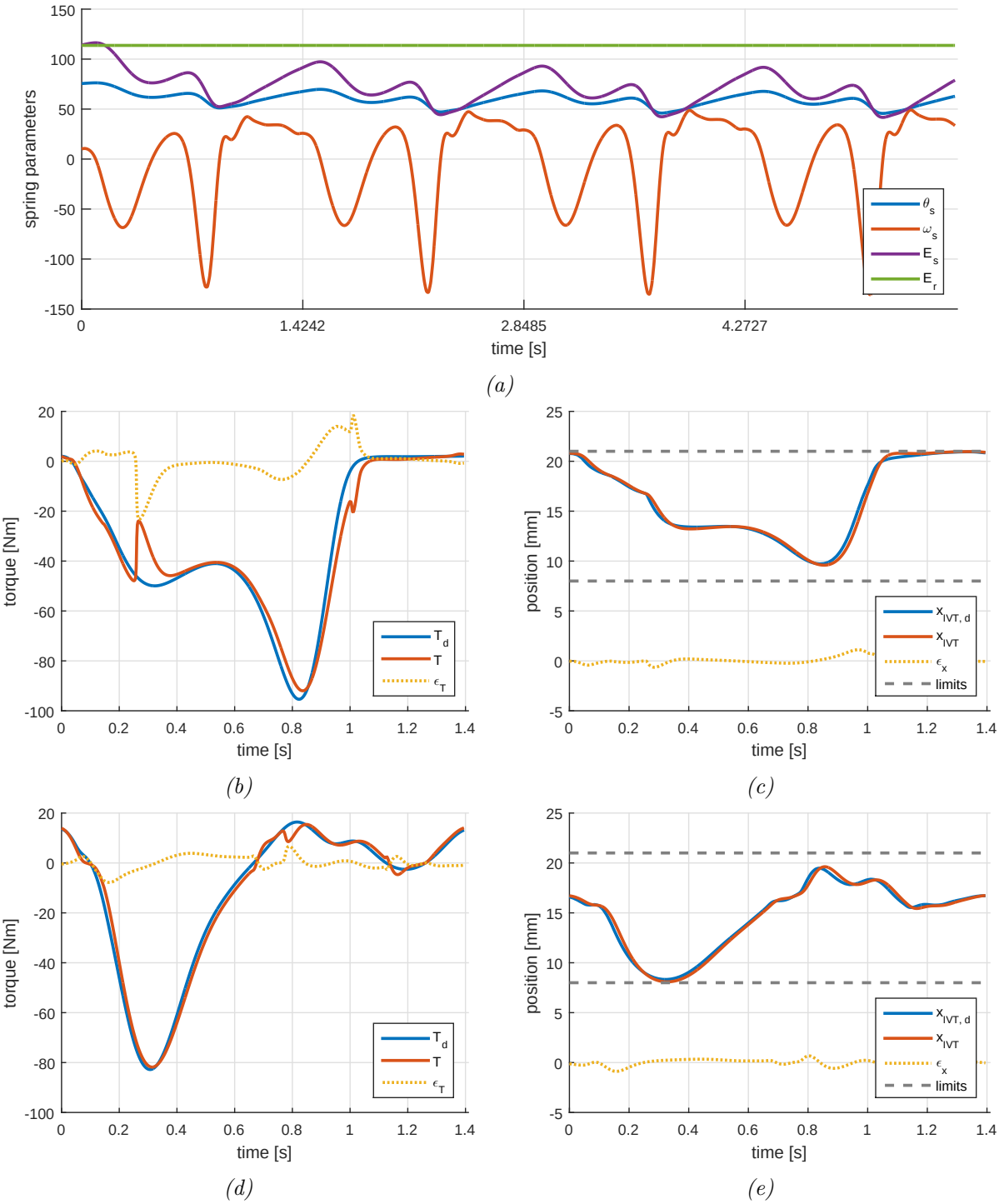

Figure 7.6: Simulation results for climbing stairs. (a) the spring measures for the first four steps starting from rest position: blue, the spring deformation angle (in rad*); red, the spring deformation angular velocity (in* rad/s*); green and purple, the spring reference energy and the spring energy (in* J*). For graphs (b) through (e), blue is the signal to track, red is the tracking, and the dotted yellow line is the error. These graphs are taken when the system has stabilised. (b) is the torque developed at the ankle joint and, (c), the position of the CVT ring in the IVT at the ankle. (d) and (e) are the same for the knee joint.*

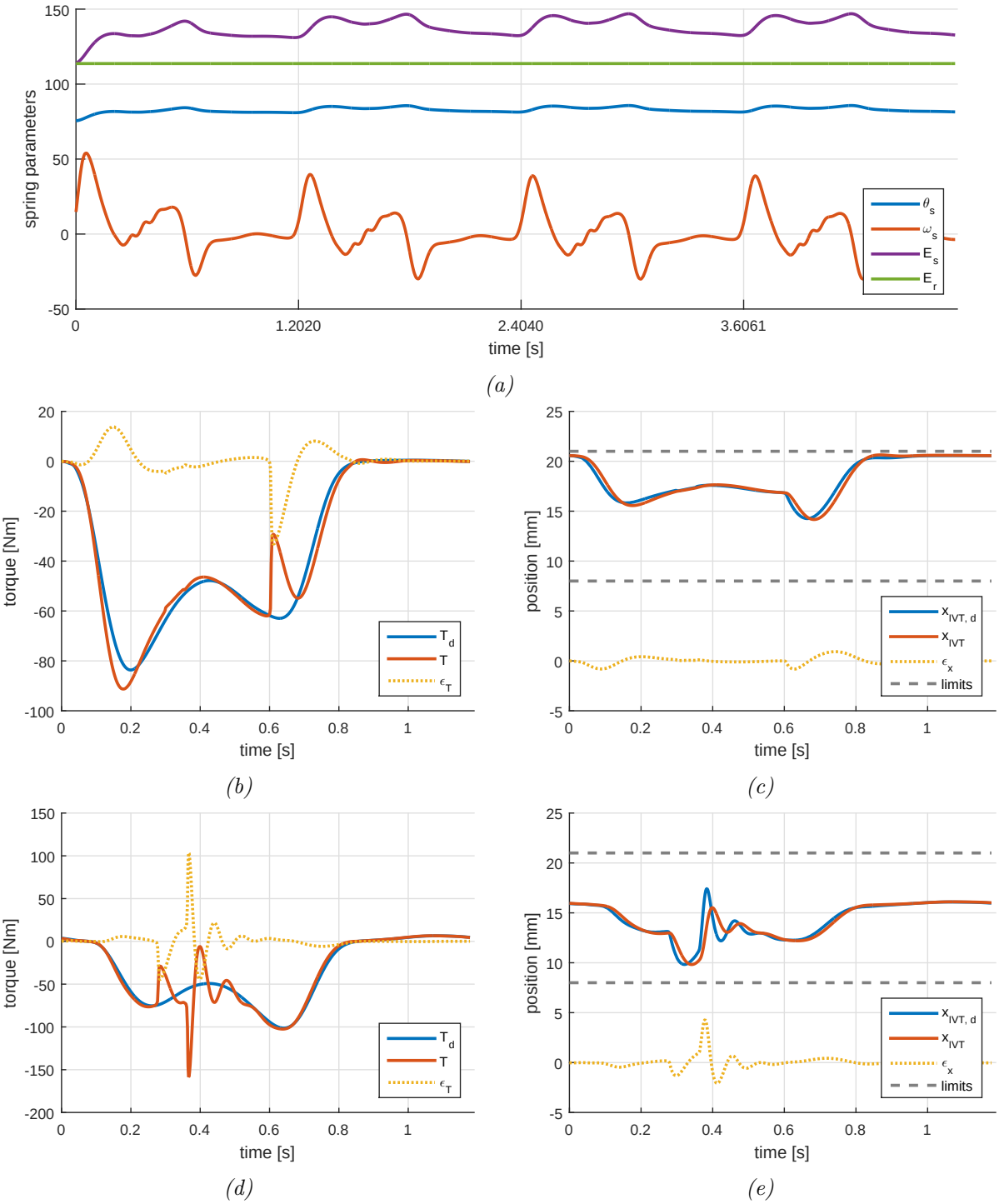

Figure 7.7: Simulation results for descending stairs. (a) the spring measures for the first four steps starting from rest position: blue, the spring deformation angle (in rad*); red, the spring deformation angular velocity (in* rad/s*); green and purple, the spring reference energy and the spring energy (in* J*). For graphs (b) through (e), blue is the signal to track, red is the tracking, and the dotted yellow line is the error. These graphs are taken when the system has stabilised. (b) is the torque developed at the ankle joint and, (c), the position of the CVT ring in the IVT at the ankle. (d) and (e) are the same for the knee joint.*

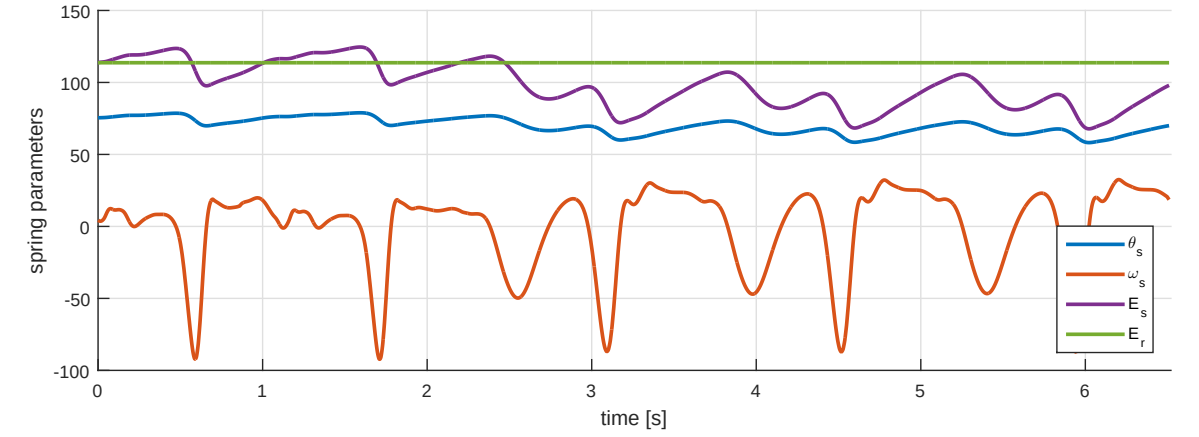

(a)

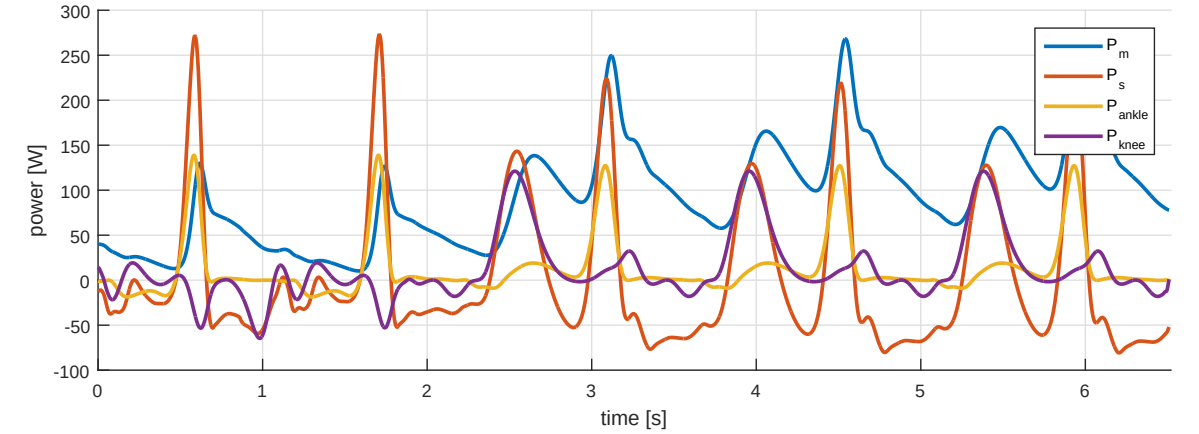

(b)

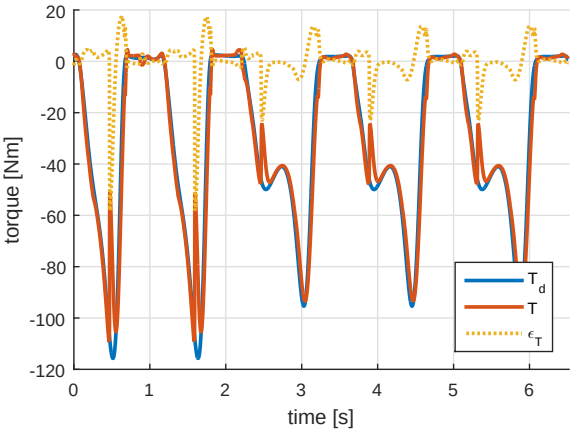

(c)

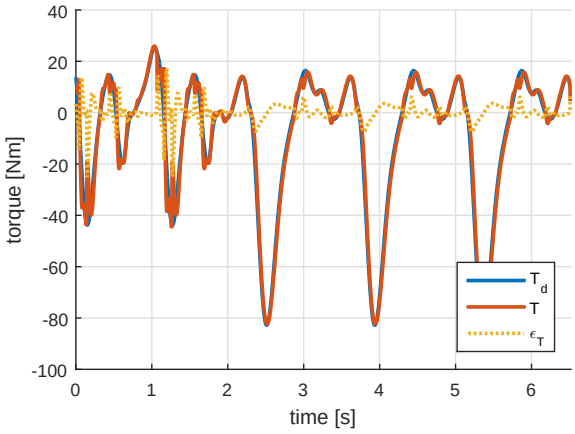

(d)

Figure 7.8: Simulation results for the transition from level ground walking to climbing stairs. First one step and one incomplete step on level ground then the transition to climbing stairs and then two more steps on the stairs. (a) the spring measures: blue, the spring deformation angle (in rad*); red, the spring deformation angular velocity (in* rad/s*); green and purple, the spring reference energy and the spring energy (in* J*). (b) powers at different stages of the mechanism (in* W*): blue, the electrical power to feed the main motor; red, the power delivered by the spring; yellow and purple, respectively, the powers required at the ankle and the knee joint. Bottom two graphs are the torques at the joints of, (c), the ankle and, (d), the knee. Blue is the desired torque, red is the produced torque at the prosthesis joint, and the dotted yellow line is the error.*

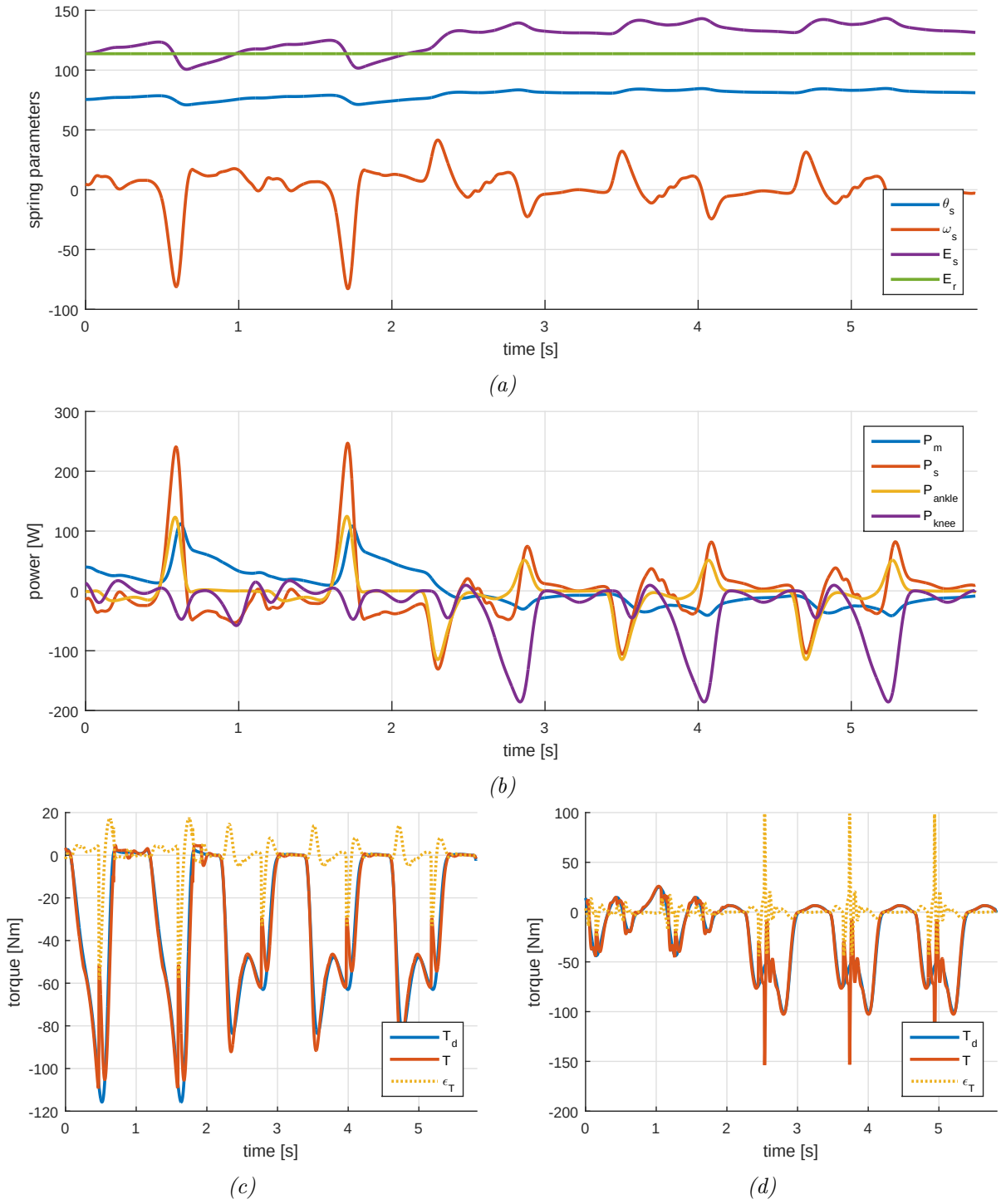

Figure 7.9: Simulation results for the transition from level ground walking to descending stairs. First one step and one incomplete step on level ground then the transition to descending stairs and then two more steps on the stairs. (a) the spring measures: blue, the spring deformation angle (in rad*); red, the spring deformation angular velocity (in* rad/s*); green and purple, the spring reference energy and the spring energy (in* J*). (b) powers at different stages of the mechanism (in* W*): blue, the electrical power to feed the main motor; red, the power delivered by the spring; yellow and purple, respectively, the powers required at the ankle and the knee joint. Bottom two graphs are the torques at the joints of, (c), the ankle and, (d), the knee. Blue is the desired torque, red is the produced torque at the prosthesis joint, and the dotted yellow line is the error.*

Chapter 8

Ankle joint dynamics during controlled dorsiflexion and powered plantar flexion

In the chapters 4 through 7 ,the dynamics of the ankle and knee joint were ignored and the torque and position profiles were taken separately from the literature. This was sufficient to study the control and energetics of the prosthesis. One of the results is that torque drops appear in torque peaks when the power flow reverses direction. In the real dynamic system, what would be the resulting impact in terms of the desired movement of the joint? And what is the behaviour of the torque profile when everything is interconnected? Indeed, in reality, the torque drop has an impact on the position, velocity and acceleration of the joint, but power, which is responsible for the torque drop, depends itself on the torque and angular velocity of the joint.

8.1 Simplified ankle model

To answer these questions, a simplified model of the ankle joint was created, it can be compared to the model in Winter et al. [29]. A schematic of the simplified model is presented in Figure 8.1. Three torques act on the ankle joint: The torque developed by the ankle joint, T_{ankl} (positive for plantar flexion); the momentum developed by the the ground reaction force, corresponding to the weight of the amputee's body (according to Newton's third law of motion), $F_r\, l \sin\theta_{ankle}$; and a viscous damping, proportional to the joint angular velocity, $B_{ankl}\, \frac{\mathrm{d}\theta_{ankle}}{\mathrm{d}t}$. According to Newton's second law of motion, the ankle joint dynamics are thus governed by the following differential equation:

$$I\, \frac{\mathrm{d}^2\theta_{ankle}}{\mathrm{d}t^2} = T_{ankle} - F_r\, l \sin\theta_{ankle} - B_{ankle}\, \frac{\mathrm{d}\theta_{ankle}}{\mathrm{d}t}, \tag{8.1}$$

with, I, the inertia of the body with respect to the ankle.

The system was further simplified with the following hypotheses:

1. The system is reduced to a single degree of freedom (the ankle) so that the differential is no longer needed.

2. We neglect the spring dynamics, assuming that a constant torque is available at the IVT input.

3. We assume that the torque to be tracked follows a sinusoidal profile. This artificial torque profile was created by looking at the previously used torque profiles from the literature and the torque drops observed in the results. The biggest torque drop (presumably the one that has the most influence on the ankle dynamics) that we encountered in this work appears in the middle of the torque peak at ankle during level ground walking. This peak rises to $\approx 120\,\mathrm{Nm}$, and the duration of one step is $\approx 1\,\mathrm{s}$. Inspired by this information,

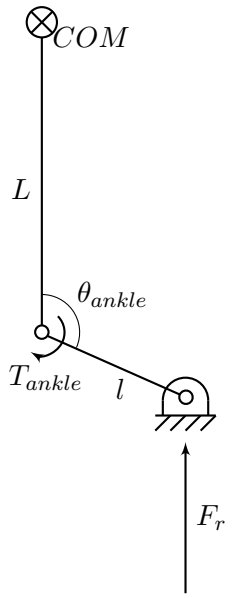

Figure 8.1: Simplified model of the ankle joint. The vertical line represents the leg with the centre of mass (COM) attached as a fixed rigid body. The oblique line represents the foot with toes fixed on the ground. Details about the symbols used is available at the List of Symbols.

the artificial torque profile was chosen to be a sinusoidal wave with a frequency of 1 Hz, oscillating between 20 Nm and 120 Nm.

4. The controller for the transmission ratio of the IVT is the same as in the previous model, as described in Section 6.3. The gain of the integral term was tuned so that time response of the system is the same as in the model of the prosthesis, i.e. 55 ms.

5. This model accounts for power losses in the IVT in the same way as in the previous model, as described in Section 6.1.2.

To investigate what would happen with more powerful motors at the IVT's, two additional cases are studied with different gains. One with a gain corresponding to a time response of the system of 13.75 ms (4 times faster). And one with a very big gain, corresponding to a time response of the system of 0.02 ms, this approaches the ideal case where the transmission ratios are adapted instantaneously. The torque developed at the motors is of course higher when the time constant goes down (see Table 8.1).

Table 8.1: Comparison of the torques that develop inside the IVT motors for different desired response times of the system during level ground walking

	Torque developped inside the IVT at the...	
response time	...ankle	...knee
$\tau = 55$ ms	16 mNm	16 mNm
$\tau = 13.75$ ms	180 mNm	160 mNm

8.2 Simulation results

The tracking of the artificial torque profile was simulated with this simplified model. The simulation was ran long enough for the system to stabilise and not to depend on the initial values. The torque at the output of the IVT, the position and derivatives in the simplified

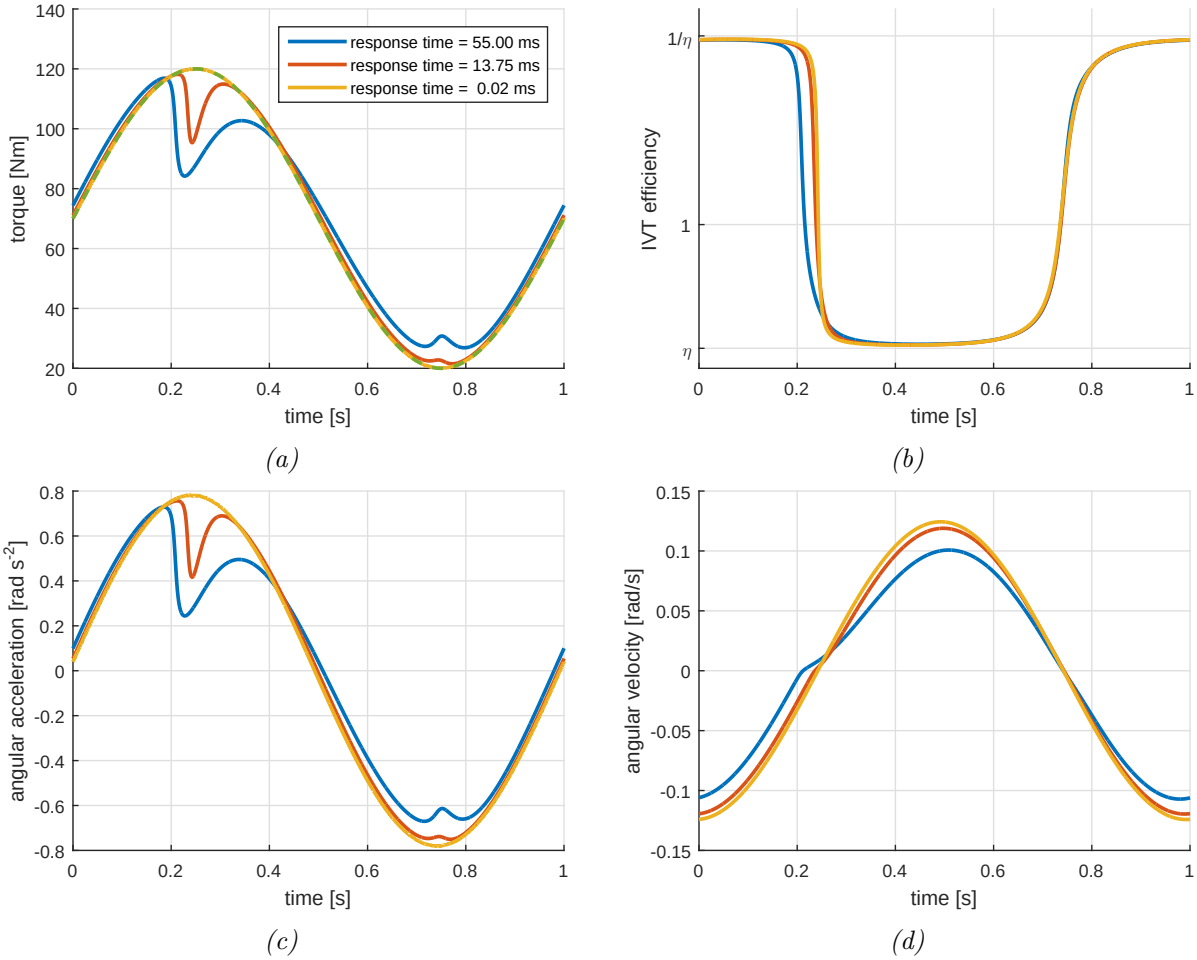

Figure 8.2: Ankle joint dynamics of the prosthesis and the effect of torque drop due to power flow reversal. IVT ratios are computed with the controller described in Section 6.3. Simulations ran for three different values for the gain of the integral term of this controller. Blue corresponding to a time response of the system of 55 ms *(same as for the other simulations); red to* 13.75 ms*; and yellow to* 0.02 ms *(for comparison with a case approaching ideal torque tracking). (a) the torque at the ankle joint, dashed green line represents the desired torque. (b) the gain on the torque representing the efficiency of the IVT. (c) the angular acceleration of the angle joint. (d) the angular velocity of the ankle joint.*

ankle model and the efficiency of the IVT where measured. The results of the simulations for one period ("artificial step") towards the end of the simulations are plotted in Figure 8.2. What happens is the following:

1. As long as the power is negative, a good tracking of torque is observed. As torque increases, the angular velocity rises from a negative value to a positive value. Up to here there is not much change with the case of the model of the prosthesis.

2. When the sign of the angular velocity changes, the power flow reverses, and the torque drop appears. This drop in torque is directly responsible for a drop in angular acceleration, which is in turn responsible for a less steep angular velocity profile. The good news is that, as the angular acceleration of the joint does not change sign, the velocity does not go down again. This means that the angle continues to increase (plantar flexion), although at a slower pace than in a healthy leg. This suggests that amputee would feel a sort of delay in the joint movement, but neither shaking nor stagnation.

3. After the drop in torque, the integral term of the controller cares compensate the induced static error, the angular acceleration increases again, and the angular velocity almost recovers its initial slope (slope before the drop in torque).

This figure reveals, that, if the prosthesis is equipped with motors capable of moving the rings of the CVT's of the IVT's 4 times faster, the delay in the angular velocity profile is significantly reduced. It would be interesting to investigate the effect of this delay (currently $\approx 0.1\,\mathrm{s}$) in terms of haptic perception to determine if this is an issue that needs to be dealt with or if the presently dimensioned motors suffice. In the ideal case of perfect torque tracking, the delay in the angular velocity profile is of course absent.

Chapter 9

Conclusions

This study describes the design of a model and controllers for a mechanism for a transfemoral 2 degree of freedom ankle-knee prosthesis. The mechanism involves the storing and releasing of energy in a spring. On one side of the spring, the main motor provides the necessary energy by winding the spring. On the other side a differential distributes the power to the two joints. At the joints, infinitely variable transmissions are used to provide the desired torque output.

Special attention was accorded to take energy losses into account in the model. These depend on the directions of the power flows in the prosthesis. The model also comprise the modelling of the dynamics of the motors that actuate the IVT's.

A control architecture was developed. It controls the prosthesis mechanism to provide a desired output torque at all times by:

- adequately choosing the transmission ratios of the IVT's;
- control the IVT actuators so that the chosen transmission ratios are obtained; and, maybe most importantly,
- control the main motor to always sufficiently rewind the spring.

The controller parameters were then tuned to minimize the total energy consumption of the prosthesis.

The model and controller were validated with experimental results. An acceptable torque tracking was achieved for all tasks (level ground walking, climbing and descending stairs, and the transition between these tasks). However, due to power flow reversals, inevitable torque drops appeared in the torque tracking profile.

The effect of these torque drops on the dynamics of the joints was then studied. It revealed a delay in the angular velocity profile but no velocity reversal nor stagnating position. In a future work it might be interesting to investigate the impact on haptic perception and on the accurate mimicking of the natural gait of such a delay in the angular velocity profile. This might help to better revisit the dimensioning of the IVT actuators.

In sum this work showed that the IVT based principle is a promising concept for transfemoral lower limb prostheses because of its low energy consumption and torque producing capabilities.

Bibliography

[1] Advanced amputee solutions llc: Amputee statistics you ought to know. http://advancedamputees.com/amputee-statistics-you-ought-know.

[2] Amputee coalition: Limb loss statistics. http://www.amputee-coalition.org/limb-loss-resource-center/resources-by-topic/limb-loss-statistics/limb-loss-statistics/.

[3] Landmine and cluster munition monitor: Issues with landmines. http://www.the-monitor.org.

[4] Maurice leblanc: Estimates of amputee population. https://web.stanford.edu/class/engr110/2011/LeBlanc-03a.pdf.

[5] N. H. Beachley and A. A. Frank. Continuously variable transmissions: Theory and practice. Master's thesis, College of Engineering, University of Wisconsin, Madison, 1979.

[6] S. M. Behrens, R. Unal, E. E. G. Hekman, R. Carloni, S. Stramigioli, and H. F. J. M. Koopman. Design of a fully-passive transfemoral prosthesis prototype. In *33rd Annual International Conference of the IEEE EMBS Boston, Massachusetts USA*, August - September 2011.

[7] R. D. Bellman, M. A. Holgate, and T. G. Sugar. Design of an active robotic ankle prosthesis with two actuated degrees of freedom using regenerative kinetics. In *Proceedings of the 2nd Biennial IEEE/RAS-EMBS International Conference on Biomedical Robotics and Biomechatronics Scottsdale, AZ, USA*, October 2008.

[8] C. Brace, M. Deacon, N. D. Vaughan, C. R. Burrows, and R. W. Horrocks. Integrated passenger car diesel cvt powertrain control for economy and low emissions. In *IMechE International Seminar S540 'Advanced Vehicle Transmissions and Powertrain Management', University of Bath*, September 1997.

[9] J. Carter, B. Pohl, B. Rutter, R. Raney, and B. Sadler. The turbo trac traction drive cvt. *Society of Automotive Engineers International*, 2004.

[10] P. Cherelle, V. Grosu, A. Matthys, B. Vanderborght, and D. Lefeber. Design and validation of the ankle mimicking prosthetic (amp-) foot 2.0. *Transactions on Neural and Rehabilitation Engineering*, 22:138 – 148, January 2014.

[11] J. R. Dormand and P. J. Prince. A family of embedded runge-kutta formulae. *Journal of Computational and Applied Mathematics*, 6:19 –26, March 1980.

[12] C. Everarts, B. Dehez, and R. Ronsse. Variable stiffness actuator applied to an active ankle prosthesis : Principle, energy-efficiency, and control. In *International Conference on Intelligent Robots and Systems (IROS), Vilamoura*, pages 323 – 328. IEEE, October 2012.

[13] C. Everarts, B. Dehez, and R. Ronsse. Novel infinitely variable transmission allowing efficient transmission ratio variations at rest. In *International Conference on Intelligent Robots and Systems (IROS), Hamburg*, pages 5844 – 5849. IEEE, September- October 2015.

[14] K. H. Ha, H. A. Varol, and M. Goldfarb. Volitional control of a prosthetic knee using surface electromyography. *Transactions on Biomedical Engineering*, 58:144 – 151, January 2011.

[15] H. M. Herr and A. M. Grabowski. Bionic ankle – foot prosthesis normalizes walking gait for persons with leg amputation. *Biological sciences*, 279:457–464, July 2011.

[16] J. Hitt, T. Sugar, M. Holgate, R. Bellman, and K. Hollander. Robotic transtibial prosthesis with biomechanical energy regeneration. *Industrial Robot: An International Journal*, 36: 441– 447, January 2014.

[17] B. E. Lawson, H. A. Varol, and M. Goldfarb. Standing stability enhancement with an intelligent powered transfemoral prosthesis. *Transactions on Biomedical Engineering*, 58: 2617 – 2624, September 2011.

[18] L. Mangialardi and G. Mantriota. Power flows and efficiency in infinitely variable transmissions. *Mechanism and Machine Theory*, 34:973 – 994, October 1999.

[19] A. Matthys, P. Cherelle, M. Van Damme, B. Vanderborght, and D. Lefeber. Concept and design of the hekta (harvest energy from the knee and transfer it to the ankle) transfemoral prosthesis. In *The Fourth IEEE RAS/EMBS International Conference on Biomedical Robotics and Biomechatronics, Roma, Italy*, June 2012.

[20] R. Riener, M. Rabuffetti, and C. Frigo. Stair ascent and descent at different inclinations. *Gait and Posture*, 15:32 – 44, 2002.

[21] L. F. Shampine and M. W. Reichelt. The matlab ode suite. *Journal on Scientific Computing*, 18:1–22, January 1997.

[22] S. Stramigioli, G. van Oort, and E. Dertien. A concept for a new energy efficient actuator. In *International Conference on Advanced Intelligent Mechatronics, Xi'an, China*, pages 671–675. IEEE, July 2008.

[23] F. Sup, H. A. Varol, J. Mitchell, T. J. Withrow, and M. Goldfarb. Self-contained powered knee and ankle prosthesis : Initial evaluation on a transfemoral amputee. In *11th International Conference on Rehabilitation Robotics Kyoto International Conference Center, Japan*, June 2009.

[24] F. Sup, H. A. Varol, and M. Goldfarb. Upslope walking with a powered knee and ankle prosthesis : Initial results with an amputee subject. *Transactions on Neural and Rehabilitation Engineering*, 19:71 – 78, February 2011.

[25] G. Tonietti, R. Schiavi, and A. Bicchi. Design and control of a variable stiffness actuator for safe and fast physical human/robot interaction. In *Proceedings of the 2005 IEEE International Conference on Robotics and Automation*, pages 526–531. IEEE, April 2005.

[26] R. Unal, F. Klijnstra, S. Stramigioli, B. Burkink, H. F. J. M. Koopman, S. M. Behrens, R. Carloni, and E. E. G. Hekman. Modeling of walkmech : a fully-passive energy-efficient transfemoral prosthesis prototype. In *IEEE International Conference on rehabilitation robotics*, 2013.

[27] H. A. Varol, F. Sup, and M. Goldfarb. Multiclass real-time intent recognition of a powered lower limb prosthesis. *Transactions on Biomedical Engineering*, 57:542 – 551, March 2010.

[28] O. Vinogradov. *Fundamentals of kinematics and dynamic of machines and mechanisms*, chapter 5.10, pages 162 – 167. CRC Press, 1998.

[29] D. A. Winter, A. E. Patla, F. Prince, M. Ishac, and K. Gielo-Perczak. Stiffness control of balance in quiet standing. *Journal of neurophysiology*, 80:1211 – 1221, April 1998.

[30] D. Yu and N. Beachley. Mechanical efficiency of differential gearing. *Gear Technology*, 3:8 – 16, 48, August 1986.

Appendix A

Data sheets

A.1 Main motor

Maxon EC-max 30 ∅30 mm, brushless, 60 W, with Hall sensors (part number 272763)

Values at nominal voltage		
	Nominal voltage	24 V
	No load speed	9340 rpm
	No load current	231 mA
	Nominal speed	8040 rpm
	Nominal torque (max. continuous torque)	60.7 mNm
	Nominal current (max. continuous current)	2.66 A
	Stall torque	458 mNm
	Stall current	18.8 A
	Max. efficiency	81 %
Characteristics		
	Terminal resistance	1.27 Ω
	Terminal inductance	0.143 mH
	Torque constant	24.3 mNm/A
	Speed constant	393 rpm/V
	Speed / torque gradient	20.6 rpm/mNm
	Mechanical time constant	4.73 ms
	Rotor inertia	21.9 gcm²

A.2 IVT motors

Maxon EC-max 16 ∅16 mm, brushless, 30 W, with Hall sensors (part number 400161)

Values at nominal voltage		
	Nominal voltage	24 V
	No load speed	42800 rpm
	No load current	185 mA
	Nominal speed	38100 rpm
	Nominal torque (max. continuous torque)	8.09 mNm
	Nominal current (max. continuous current)	1.68 A
	Stall torque	82.7 mNm
	Stall current	15.6 A
	Max. efficiency	80 %
Characteristics		
	Terminal resistance	1.53 Ω
	Terminal inductance	0.102 mH
	Torque constant	5.29 mNm/A
	Speed constant	1810 rpm/V
	Speed / torque gradient	524 rpm/mNm
	Mechanical time constant	2.93 ms
	Rotor inertia	0.534 gcm²

Appendix B

Planetary gears

Adapted from Vinogradov [28].

An elementary planetary gear train is shown in Figure B.1. The blue gear is called the sun (or central) gear, the red gear is called the planetary (or epicyclic) gear, the yellow link is called the planet carrier (or crank arm) and the green gear is called the annular gear (or annulus).

Note this system has two degrees of freedom which means that if only one velocity is given, the motion of the other elements cannot be determined. But when either the sun, the planet carrier or the annulus is held fixed, the number of degrees of freedom of this system reduces to 1. For instance if the annular gear is fixed, for a given velocity ω_{su} there is a unique velocity ω_{ca}.

Planetary gear trains allow obtaining high transmission ratios in a compact design, which makes them suitable for applications in, for example, machine tools, hoists, and automatic transmissions.

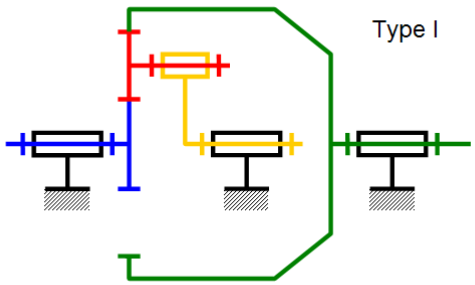

Figure B.1: Kinematic diagram of a planetary gear train. From [Creative Commons Attribution-Share Alike 3.0 Unported]

B.1 Transmission ratio

Lets start with a planetary gear train without the annulus. One can determine the transmission ratio for a planetary train. Suppose that the arm rotates with angular velocity ω_{ca}. Then, if an observer is sitting on this arm, for this observer the rotation of the sun and the planet will not be different from that for a parallel fixed-shaft system, and the corresponding transmission ratio will be ω_{pl}/ω_{su}. One realizes that an observer on the arm sees rotation in a moving (rotating) coordinate system. Now if the observer is standing on the frame, then the observer will see that the arm rotates with ω_{ca}. The question is what will be the angular velocities of gears 2 and 4 with respect to the observer on a frame. The answer is given by a general rule for summation of angular velocities in the case when a body rotates with respect to its own axis with velocity ω^1, while the axis itself rotates with respect to another axis with the velocity ω. In the case

when the two axes are parallel, the total angular velocity equals the algebraic sum of velocities of two rotations. Thus, the total angular velocity will be

$$\omega_{total} = \omega + \omega^1. \tag{B.1}$$

The above rule is directly applicable to the planetary gear trains. Indeed, the axes of the sun and the planet are parallel and one of them rotates with respect to the other with ω_{ca}. Now, the transmission ratio in a coordinate system rotating with ω_{ca} is known. It is equal to $-N_{su}/N_{pl}$. Thus, if one applies a counter-rotation with $-\omega_{ca}$ to the entire system, then the gear velocities (according to the rule of summation) will be $\omega_{pl} - \omega_{ca}$ and $\omega_{su} - \omega_{ca}$, and the planet carrier link becomes fixed. Thus, the transmission ratio is given by:

$$\frac{\omega_{pl} - \omega_{ca}}{\omega_{su} - \omega_{ca}} = -\frac{N_{su}}{N_{pl}}. \tag{B.2}$$

The case with no annulus described by Equation (B.2) is equivalent to a one-pair system in conventional gear trains. In this respect, the full system with annulus in Figure B.1 is equivalent to a two-pair system where the pairs are functionally in series with each other. Thus, in this case there are two transmission ratios: first, from the sun gear to the planetary gear, which is described by Equation (B.2), and, second, from the planetary gear to the annular gear. The latter is equal to (in a rotating coordinate system)

$$\frac{\omega_{an} - \omega_{ca}}{\omega_{pl} - \omega_{ca}} = \frac{N_{pl}}{N_{an}}. \tag{B.3}$$

Note that the plus sign on the right-hand side in Equation (B.3) is due to internal gear meshing. If $\omega_{an} = 0$ (annular gear is fixed) and ω_{su} is known, then ω_{ca} and ω_{pl} are found from equations (B.2) and (B.3).

And, finally, it should be noted that the planetary gear plays the role of an idle gear. Indeed, the total transmission ratio for a system in series is equal to the product of transmission ratios of its subsystems. In this case the total transmission ratio is thus the product of equations (B.2) and (B.3). The result is

$$\frac{\omega_{an} - \omega_{ca}}{\omega_{su} - \omega_{ca}} = -\frac{N_{su}}{N_{an}} \tag{B.4}$$

As one can see, the angular velocity ω_{pl} of the planetary gear does not affect the transmission ratio.

The above equation confirms that the system shown in Figure B.1 has two degrees of freedom. Indeed, if, for instance, only ω_{su} is given, two unknown velocities remain, ω_{ca} and ω_{an}, while the gears are defined. But if either the sun, the planet carrier or the annulus is held fixed, the relation between the velocities of the two other elements can be obtained. For instance:
Given that $\omega_{an} = 0$ and ω_{su} is known, the unknown velocity ω_{ca} can be immediately found from Equation (B.4):

$$\omega_{ca} = \omega_{su} \frac{\dfrac{N_{su}}{N_{an}}}{1 + \dfrac{N_{su}}{N_{an}}}. \tag{B.5}$$

B.2 Torque ratios

In planetary gear trains, two speeds must be known, in order to determine the third speed. However, in a steady state condition, only one torque must be known, in order to determine

the other two torques. The equations which determine torque are:

$$\begin{cases} T_{an} = T_{su} \dfrac{N_{an}}{N_{su}} & \text{(B.6)} \\ T_{an} = T_{ca} \dfrac{N_{an}}{N_{an} + N_{su}} & \text{(B.7)} \\ & \text{(B.8)} \end{cases}$$

$$\begin{cases} T_{ca} = T_{an} \dfrac{N_{an} + N_{su}}{N_{an}} & \text{(B.9)} \\ T_{ca} = T_{su} \dfrac{N_{an} + N_{su}}{N_{su}} & \text{(B.10)} \\ & \text{(B.11)} \end{cases}$$

$$\begin{cases} T_{su} = T_{an} \dfrac{N_{su}}{N_{an}} & \text{(B.12)} \\ T_{su} = T_{ca} \dfrac{N_{su}}{N_{an} + N_{su}} & \text{(B.13)} \\ & \text{(B.14)} \end{cases}$$

Appendix C

CAD drawings of the actual CVT prototype

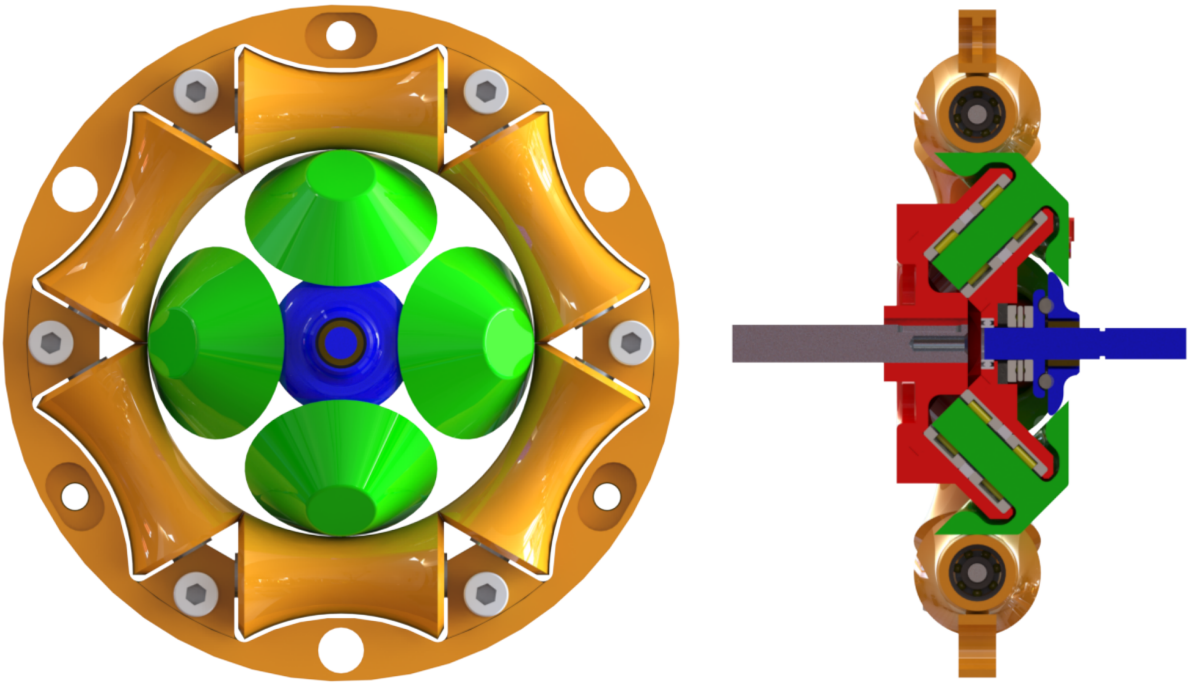

(a) Facing the ring *(b) Cut through view.*

Figure C.1: CVT ring with planets, planet carrier and sun. The rollers are depicted in orange, the conical planets in green, the plant carrier in red and the sun in blue.

(a) CVT planet carrier

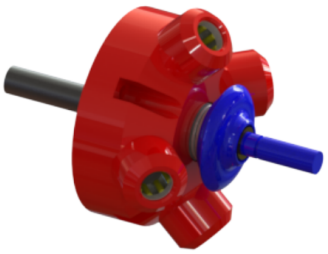

(b) CVT sun

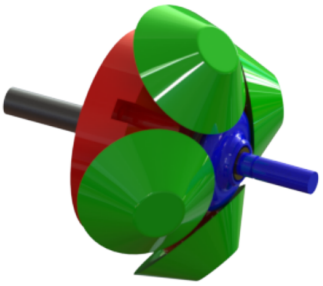

(c) CVT cones

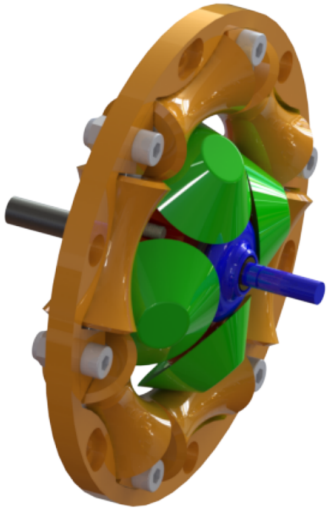

(d) CVT ring

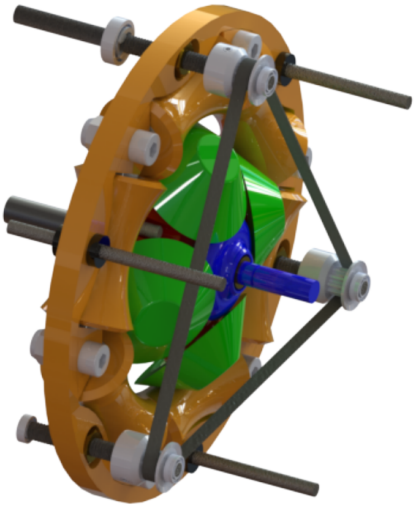

(e) CVT ring actuation

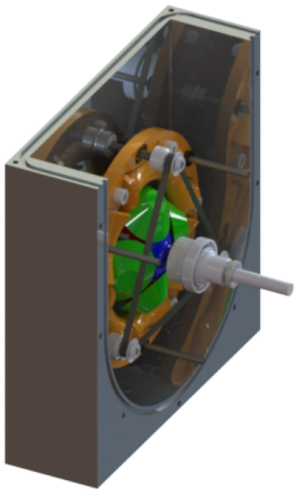

(f) CVT frame

Figure C.2: Sequential assembly of the CVT CAD

Rue Archimède, 1 bte L6.11.01, 1348 Louvain-la-Neuve **www.uclouvain.be/epl**